JOURNAL OF THE AMERICAN CHEMICAL SOCIETY

pubs.acs.org/JACS

Article

Substituent and Heteroatom Effects on $\pi-\pi$ Interactions: Evidence That Parallel-Displaced π-Stacking is Not Driven by Quadrupolar Electrostatics

Brandon Schramm,[†] Montgomery Gray,[†] and John M. Herbert*

Cite This: *J. Am. Chem. Soc.* 2025, 147, 3243−3260

Read Online

ACCESS | Metrics & More | Article Recommendations | Supporting Information

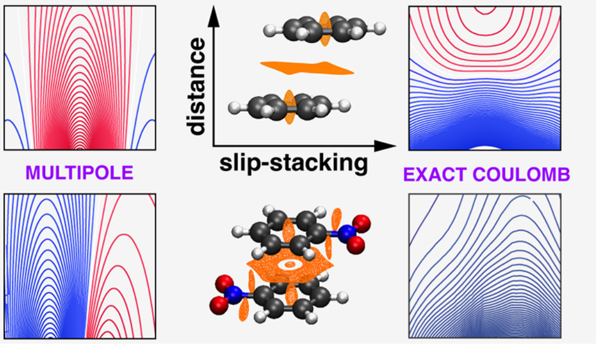

ABSTRACT: Stacking interactions are a recurring motif in supramolecular chemistry and biochemistry, where a persistent theme is a preference for parallel-displaced aromatic rings rather than face-to-face π-stacking. This is typically explained in terms of quadrupole−quadrupole interactions between the arene moieties but that interpretation is inconsistent with accurate calculations, which reveal that the quadrupolar picture is qualitatively wrong. At typical π-stacking distances, quadrupolar electrostatics may differ in sign from an exact calculation based on charge densities of the interacting arenes. We apply symmetry-adapted perturbation theory to dimers composed of substituted benzene and various aromatic heterocycles, which display a wide range of electrostatic interactions, and we investigate the interplay of Pauli repulsion, dispersion, and electrostatics as it pertains to parallel-displaced π-stacking. Profiles of energy components along cofacial slip-stacking coordinates support a prominent role for the "van der Waals model" (dispersion in competition with Pauli repulsion), even for polar monomers where electrostatic interactions are significant. While electrostatic interactions are necessary to explain the optimal face-to-face π-stacking distance and to account for the relative orientation of one polar arene with respect to another, we find no evidence to support continued invocation of quadrupolar electrostatics as a basis for π-stacking. Our results suggest that a driving force for offset-stacking exists even in the absence of electrostatic interactions. Consequently, tuning electrostatics via functionalization does not guarantee that slip-stacking can be avoided. This has implications for rational design of soft materials and other supramolecular architectures.

1. INTRODUCTION

Aromatic π-stacking is a key supramolecular motif,[1−9] yet the fundamental intermolecular forces that contribute to $\pi-\pi$ interactions continue to be debated.[10−24] A recurring question is whether these forces constitute a unique type of intermolecular interaction that is distinct from "ordinary" dispersion.[13−16] Electronic structure calculations suggest that π-stacking is driven by dispersion but enhanced by the planar geometries of aromatic moieties,[14−16] in what has been called the "pizza-π" model for stacking.[16] This is consistent with the existence of stacking interactions between molecules that are planar but not aromatic.[25−30] A key aspect of the pizza-π model is that electrostatic interactions are attractive between cofacial arenes at typical π-stacking distances (face-to-face separations R = 3.4−3.8 Å). This is supported by detailed calculations[16−20,31−34] but is inconsistent with the quadrupolar electrostatics model that is typically used to discuss $\pi-\pi$ interactions,[30,35] in which the electrostatic interaction between arene moieties is considered to be dominated by their molecular quadrupole moments.

A persistent feature of those interactions is "slip-stacking", whereby two arene moieties adopt a parallel-displaced geometry as illustrated for the benzene dimer in Figure 1. In $(C_6H_6)_2$, the energetic preference for offset-stacking is ≈1 kcal/mol,[36] but it is considerably larger in polycyclic aromatic hydrocarbons (PAHs).[16,37−39] Moreover, the parallel-displaced motif is observed repeatedly in other $\pi-\pi$ systems: between aromatic side chains in protein crystal structures;[1,2,28,40] in metal complexes with aromatic ligands;[41] in dimers of pyridinoids,[42] macrocycles,[21,43] and circumcoronenes;[44−46] for aromatic and antiaromatic π systems atop graphene;[16,19,26] and in layered materials such as covalent organic frameworks.[21,47−53] Understanding the intermolecular forces that

Received: September 23, 2024
Revised: January 2, 2025
Accepted: January 7, 2025
Published: January 17, 2025

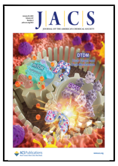

https://doi.org/10.1021/jacs.4c13291

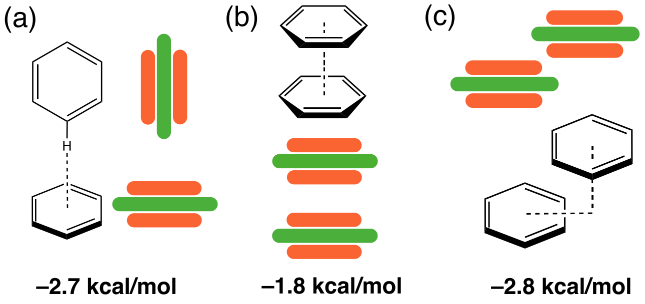

Figure 1. Canonical configurations of the benzene dimer along with cartoon representations of their charge distributions: (a) T-shaped or CH⋯π orientation, (b) cofacial "sandwich" arrangement, and (c) parallel-displaced configuration, also known as the slipped- or offset-stacked geometry. Benchmark interaction energies are D_e values from ref 36.

drive offset π-stacking is crucial for achieving rational synthetic control of these and other supramolecular architectures.[54−63]

A simple explanation for why the parallel-displaced geometry of $(C_6H_6)_2$ is lower in energy than the cofacial "sandwich" arrangement was put forward long ago by Hunter and Sanders,[64] using a potential energy model consisting of van der Waals (vdW) interactions plus electrostatics,

$$E_{\mathrm{vdW+elst}} = E_{\mathrm{vdW}} + E_{\mathrm{elst}} \tag{1}$$

In the original Hunter-Sanders model, E_{vdW} consisted of atom−atom repulsion and dispersion potentials while electrostatics (E_{elst}) was represented using point charges positioned to reproduce the benzene monomer's quadrupole moment, including out-of-plane charges.[64] Qualitatively, slip-stacking emerges from this model because dispersion is most attractive in the face-to-face geometry but electrostatics (as computed using the Hunter-Sanders point-charge model) is repulsive in that configuration. This is suggested by the cartoon charge distributions in Figure 1, versions of which can still be found in contemporary reviews.[35] Ultimately, however, we will argue that these cartoons are misleading with regard to the origins of offset π-stacking.

The atomistic model of Hunter and Sanders would later be adapted by others into a force field for aromatic moieties,[65] but Hunter and co-workers went in a different direction beginning in 2001.[2] Seizing upon benzene's sizable quadrupole moment,[66] they emphasized a picture in which substituents modulate stacking interactions by means of how they affect the π-electron density.[67] According to this quadrupolar electrostatics picture, offset π-stacking arises because quadrupole−quadrupole interactions in $(C_6H_6)_2$ are attractive in the edge-to-face geometry but repulsive in the face-to-face orientation, so slip-stacking reduces unfavorable quadrupole−quadrupole repulsion. That point of view continues to be emphasized in recent reviews.[30,35]

In contemporary literature, the term "Hunter-Sanders model" is often synonymous with quadrupolar electrostatics,[23,24,29,35,68−77] despite the presence of a repulsive term in eq 1 and notwithstanding the fact that the original Hunter-Sanders model used point charges (not quadrupoles), in order to separate π−π interactions from σ−π interactions.[64] In other recent literature, the phrase "Hunter-Sanders" is invoked as a kind of talisman, to signify that π−π interactions are understood. In what follows, we avoid the phrase "Hunter-Sanders model" due to its ambiguous meaning in contemporary literature. By "quadrupolar electrostatics model", we mean the idea that the preference for parallel-displaced π-stacking originates in quadrupole−quadrupole repulsion between cofacial arenes. The same model posits that the T-shaped (edge-to-face) benzene dimer arises due to attractive quadrupolar electrostatics. Both of these ideas are wrong.

By any name, the notion that π−π interactions are controlled by competition between quadrupolar electrostatics and dispersion has been assimilated into the lore of supramolecular organic chemistry,[35] despite limited experimental evidence.[78−82] That evidence consists mostly of correlations between substituent Hammett parameters and relative stacking energies ($\Delta\Delta G°$), measured in chemical double-mutant experiments.[79−81] Other experimental results have been ambiguous or contradictory,[83−94] nevertheless π-stacking continues to be discussed in terms of quadrupolar interactions between arenes.[13,22,29,30,76,95−122]

Rather than taking the arene's quadrupole moment as the basis for π−π interactions, Wheeler and co-workers have shown that substituent effects on stacking energies are better understood using a "direct interaction model",[12,123−127] in which through-space interaction between the substituent and the opposite arene is more important than a substituent's effect on the π-electron density of its own aromatic ring. This idea has antecedents in the through-space "polar-π" model of Cozzi and Siegel,[128−133] the evidence for which also consists of correlations between $\Delta\Delta G°$ and Hammett parameters for the substituents.[129−133] Cozzi and Siegel argued that the polar-π model is consistent with intuition regarding electron donating or withdrawing effects,[128] although Wheeler and Houk have shown how intuition can be subverted by the spatial orientation of substituent moieties.[123,134] The direct-interaction model has garnered support from experiment,[87−93] and has been confirmed at various levels of *ab initio* theory,[127,135−137] whereas *ab initio* support for a quadrupolar model of ion−π interactions is also lacking.[138,139]

Quadrupolar electrostatics is routinely used to explain the prevalence of offset π-stacking[35,43] but we have suggested that slip-stacking is better understood in terms of vdW interactions, i.e., as a competition between dispersion and Pauli repulsion.[16−19] In our view, this provides a more satisfying explanation for the ubiquitous nature of parallel-displaced π-stacking in protein crystal structures,[40] because those short-range forces are ever-present despite differences in long-range electrostatics engendered by myriad protein environments.[16,17] This prediction was recently confirmed in a broad computational survey of π−π interactions in proteins.[24]

Elucidating the driving forces behind offset-stacking has numerous implications for chemical science. For example, slip-stacking may be detrimental to catalysis applications in covalent organic frameworks, as it might occlude the pores. In organic photovoltaic or optoelectronic materials, offset-stacking may enhance electrical conductivity and/or exciton delocalization,[45,56,63] yet conductivity is exquisitely sensitive to the interlayer spacing.[140] For these reasons, it is important to know whether offset-stacking is tunable using electron donating or withdrawing groups.[52]

This question is examined in the present work via detailed study of the energy components that contribute to π−π interactions in substituted benzene dimers and in dimers composed of aromatic heterocycles. What emerges is a more nuanced explanation for offset π-stacking as compared to our previous attribution based on E_{vdW}.[16−19,21] Here, we show that electrostatics plays an important role in determining the optimal face-to-face separation of two arene moieties, even while Pauli repulsion and dispersion together are enough to elicit a lateral offset. As in the pizza-π model,[16] a key aspect of this analysis is that the quadrupolar electrostatics picture is extremely misleading. The exact electrostatic interaction energy,

$$E_{\mathrm{elst}} = \int \frac{\rho_{\mathrm{A}}(\mathbf{r}_1)\rho_{\mathrm{B}}(\mathbf{r}_2)}{\|\mathbf{r}_1 - \mathbf{r}_2\|} \mathrm{d}\mathbf{r}_1 \mathrm{d}\mathbf{r}_2 \tag{2}$$

computed using isolated-monomer charge densities $\rho_{\mathrm{A}}(\mathbf{r})$ and $\rho_{\mathrm{B}}(\mathbf{r})$ that include both nuclei and electrons, may differ in sign as compared to an approximation based on the monomer dipole and quadrupole moments. Even multicenter (distributed) multipole expansions may not correct this deficiency at typical π-stacking distances,[31] where $\rho_{\mathrm{A}}(\mathbf{r})$ and $\rho_{\mathrm{B}}(\mathbf{r})$ interpenetrate significantly. As such, low-order molecular multipole moments should not be employed—even conceptually—to understand π-stacking at vdW contact distances. At those length scales, charge penetration can lead to electrostatic attraction, even in geometries where the quadrupole−quadrupole interactions are repulsive.[11,16−20] Inclusion of higher-order multipole moments (e.g., using atomic or otherwise distributed multipoles) may not rectify these qualitative deficiencies.[31]

2. COMPUTATIONAL METHODS

As in previous work on $\pi-\pi$ interactions,[16−19,21] we employ the methods of extended symmetry-adapted perturbation theory (XSAPT)[19] to profile the total intermolecular interaction energy (E_{int}) and its components,

$$E_{\mathrm{int}} = E_{\mathrm{elst}} + E_{\mathrm{exch}} + E_{\mathrm{ind}} + E_{\mathrm{disp}} \tag{3}$$

These components include electrostatics (E_{elst}), exchange or Pauli repulsion (E_{exch}), induction (E_{ind}), and dispersion (E_{disp}).[18,141−143] The induction energy contains both polarization and charge transfer,[144−147] which we have not separated because E_{ind} is numerically small and qualitatively unimportant for the systems examined here.

XSAPT is a hybrid approach with foundations in perturbation theory, yet it models dispersion in nonperturbative ways that achieve benchmark-level accuracy at low cost.[148−150] The first three components in eq 3 (E_{elst}+ E_{exch}+ E_{ind}) are computed using second-order SAPT based on Kohn−Sham orbitals, as detailed elsewhere.[19,149,151] In particular, E_{elst} is the exact Coulomb interaction between isolated-monomer charge densities,[18,143] including both nuclei and electrons (eq 2).

The dispersion energy cannot be modeled accurately using second-order perturbation theory.[150−153] Higher-order SAPT does achieve benchmark accuracy,[153] but at prohibitive $\mathcal{O}(N^7)$ cost.[153−155] As an alternative, XSAPT exploits the inherent separability of eq 3 to substitute a many-body dispersion (MBD) model for E_{disp}.[156−158] The result is hybrid method called XSAPT + MBD,[19,157−159] which achieves sub-kcal/mol accuracy (for both E_{int} and its components) with respect to the best *ab initio* benchmarks.[158−160] Unlike energy decompositions based on density-functional theory (DFT), where dispersion can be difficult to disentangle from semilocal exchange and correlation,[161−163] the XSAPT + MBD energy components are in good agreement with reliable third-order SAPT calculations.[160,163] As such, the decomposition in eq 3 does not benefit from error cancellation,[160] and the definition of E_{disp} is less ambiguous in XSAPT + MBD as compared to DFT-based energy decomposition analyses.[163]

All calculations were performed using Q-Chem.[164] Additional details can be found in the Supporting Information, including a more complete description of the XSAPT + MBD approach and the composite triple-ζ basis set that was used.

3. RESULTS AND DISCUSSION

3.1. Offset-Stacking in Benzene Dimer.

To introduce how slip-stacking can emerge without an electrostatic driving force, we first consider $(\mathrm{C_6H_6})_2$. This system has long been regarded as an archetypal example of π-stacking although it is an outlier among PAHs.[16] Already for naphthalene dimer, and increasingly for larger acene dimers, parallel-displaced π-stacking is significantly more stable as compared to edge-to-face CH⋯π interactions,[14,16,38] whereas for benzene dimer these two arrangements are very close in energy,[36] as indicated in Figure 1. The energy difference in larger PAHs is driven by electrostatics,[16] but the lateral offset is not.[16−19] Because $(\mathrm{C_6H_6})_2$ establishes a baseline for evaluation of substituent and heteroatom effects, we begin with a brief review of the "vdW picture" of π-stacking (Section 3.1.1), then consider how electrostatics modulates the face-to-face separation (Section 3.1.2).

3.1.1. Lateral Displacements. Figure 2 shows energy components for benzene dimer in a cofacial arrangement, along a sliding coordinate that corresponds to offset-stacking. This analysis is performed separately at face-to-face distances R = 3.4 and 3.8 Å, the smaller of which is consistent with the parallel-displaced minimum-energy structure in Figure 1c while the larger separation corresponds to the D_{6h} "sandwich"

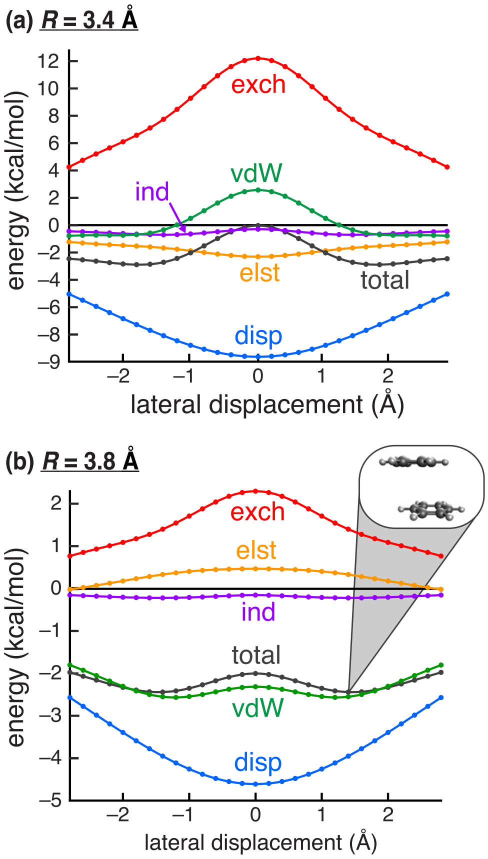

Figure 2. Energy component profiles for $(\mathrm{C_6H_6})_2$ along a cofacial sliding coordinate at face-to-face separations (a) R = 3.4 Å and (b) R = 3.8 Å, consistent with the parallel-displaced energy minimum (Figure 1c) in the former case and with the D_{6h} "sandwich" saddle point (Figure 1b) at the longer separation.

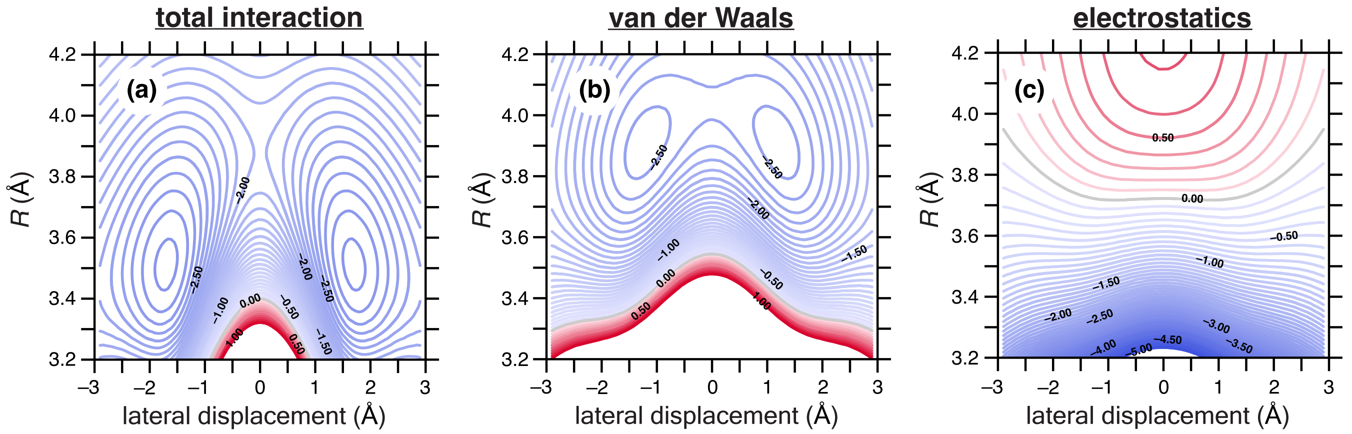

Figure 3. Two-dimensional energy contours for $(C_6H_6)_2$ along a lateral displacement coordinate and a face-to-face-separation coordinate (R), equal to the distance between the planes defined by the two coplanar monomers. The energy components that are plotted are (a) the total interaction, E_{int}; (b) $E_{vdW} = E_{exch} + E_{disp}$; and (c) the electrostatic energy, E_{elst}. Contours are drawn at intervals of 0.1 kcal/mol and labeled at intervals of 0.5 kcal/mol. Blue contours indicate attractive (negative) energy components and red contours are repulsive (positive).

structure in Figure 1b.[17,36] The D_{6h} configuration is a saddle point between equivalent parallel-displaced minima.[33]

At R = 3.4 Å, which is roughly the sum of nonbonded contact radii for two carbon atoms,[165] exact electrostatics is attractive in the cofacial arrangement ($E_{elst} < 0$), despite the fact that the quadrupole−quadrupole interaction is repulsive in cofacial geometries. In fact, even a 32-pole distributed atomic multipole calculation is strictly repulsive, at all values of R, for two coplanar benzene molecules.[34] In contrast, exact electrostatics is (slightly) repulsive at R = 3.8 Å (Figure 2b), consistent with the multipolar picture. Distributed-multipole analysis at R = 3.8 Å has been used to justify the quadrupolar electrostatics picture of π-stacking,[166] yet that distance lies (just) outside of typical vdW contact distances. (The interlayer separation in graphene is 3.35 Å, for example.[167]) Furthermore, at R = 3.8 Å a distributed multipole calculation is not yet converged to exact electrostatics.[34] Finally, electrostatic repulsion characterizes less than 3% of $\pi-\pi$ contacts in proteins.[24] Thus, any universal explanation for $\pi-\pi$ interactions needs to encompass distances $R \approx 3.4$ Å, in addition to larger distances where the quadrupolar picture is qualitatively correct.

Despite a change in sign for E_{elst}, slip-stacking is observed at both R = 3.4 and 3.8 Å, with offsets of 1.4 and 1.8 Å, respectively. At R = 3.8 Å, where the quadrupolar picture is valid, the electrostatic penalty for π-stacking is indeed reduced by displacement along a parallel sliding coordinate (Figure 2b). The effect is small, however, because $E_{elst} < 0.5$ kcal/mol even in the sandwich configuration where it is maximally repulsive. Meanwhile, the total interaction energy profile (E_{int}) is a good match to the vdW potential,

$$E_{vdW} = E_{exch} + E_{disp} \tag{4}$$

This analysis suggests that offset-stacking can be driven by a competition between short-range forces, namely, Pauli repulsion and dispersion. Longer-range electrostatic interactions are not required, contra previous claims that the orientation dependence of $(C_6H_6)_2$ is controlled by long-range interactions.[168]

The vdW potential is a qualitative match to E_{int} at both R = 3.4 Å, where charge penetration makes the electrostatic interaction attractive, but also at R = 3.8 Å where the quadrupolar picture holds and $E_{elst} > 0$. Charge-transfer effects would appear in E_{ind} so these must be negligible, consistent with previous analyses.[128,130,168,169] At smaller face-to-face distances such as R = 3.4 Å, the electrostatic term is not only attractive but also (weakly) favors the sandwich geometry, opposite to the quadrupolar picture. Only E_{vdW} is able to rationalize offset-stacking at both R = 3.4 Å and R = 3.8 Å. In previous work, we have shown that this conclusion can also be reached using alternative forms of energy decomposition analysis based on DFT calculations.[17]

3.1.2. Distance Considerations. The sign change in E_{elst} between R = 3.4 and 3.8 Å suggests it may be important to consider the face-to-face separation alongside the lateral displacement coordinate. Indeed, the use of one-dimensional scans at fixed R has recently been criticized by Cabaleiro-Lago and co-workers,[23] who instead report SAPT calculations using relaxed potential energy scans where the value of R is optimized at each lateral displacement. Those calculations suggest a dominant role for electrostatics, and the authors note that E_{exch} and E_{disp} largely cancel.[23] However, $|E_{elst}|$ is relatively small for the unsubstituted benzene dimer, in comparison to either E_{exch} or $|E_{disp}|$, and any significant imbalance between these much larger energy components would indicate that the system is far from a minimum-energy configuration. As such, our view is that near-cancellation of dispersion and Pauli repulsion simply reflects the fact that the dimer is close to a minimum-energy structure. This is certainly true for all the $(C_6H_6)_2$ configurations in Figure 1 (and nearby configurations), whether or not they constitute proper local minima on the potential energy surface.

To put this differently, consider that R = 3.8 Å is the optimal face-to-face separation for the D_{6h} sandwich geometry, which is a saddle point between symmetry-equivalent parallel-displaced local minima that are characterized by R = 3.4 Å.[17,33] This difference can be rationalized as follows. Starting from the sandwich geometry, lateral displacement reduces E_{exch} and this allows the system to access smaller face-to-face separations. By doing so, the effect of electrostatics is enhanced because $E_{elst} < 0$ at these smaller values of R. Thus, the relaxed potential scans considered by Cabaleiro-Lago et al.[23] necessarily suggest a larger role for electrostatics, but this is not inconsistent with the analysis in Section 3.1.1.

To examine this issue in more detail, Figure 3 plots two-dimensional scans of E_{int}, E_{vdW}, and E_{elst} as a function of both R

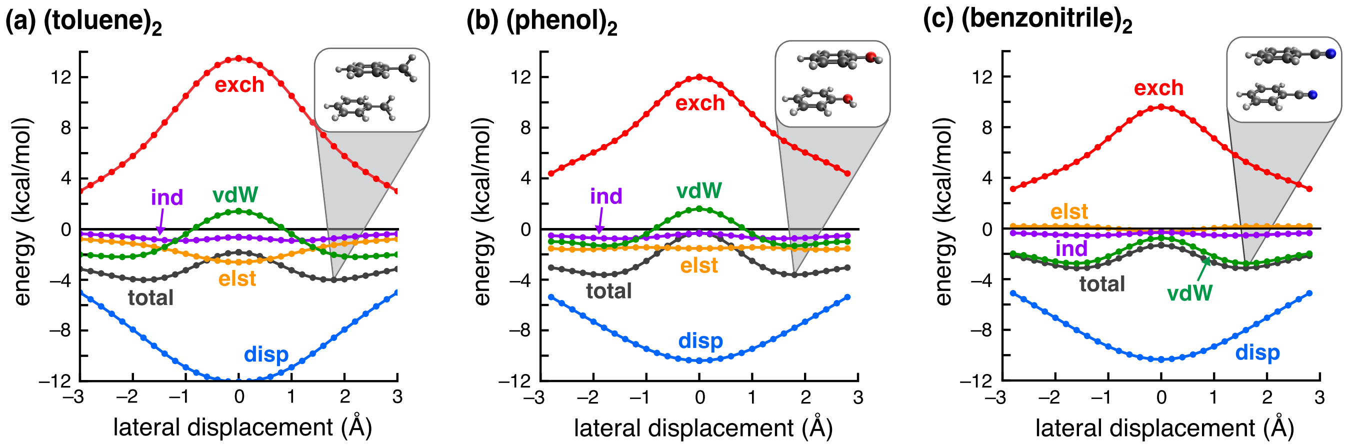

Figure 4. Energy component profiles for lateral displacement along the C−X axis in $(C_6H_5X)_2$ dimers: (a) toluene at R = 3.5 Å, (b) phenol at R = 3.4 Å, and (c) benzonitrile at R = 3.5 Å. In each case, the face-to-face separation R is consistent with the parallel-displaced energy minimum.

and the lateral displacement coordinate considered previously. (The scans in Figure 2 are one-dimensional cuts through the surfaces in Figure 3, at either R = 3.4 or 3.8 Å.) Comparing E_{vdW} in Figure 3b to E_{int} in Figure 3a, it is evident that the vdW potential would generate an offset of approximately 1.25 Å, if left to its own devices, but would place the minimum-energy cofacial geometry at $R \approx 3.9$ Å. Considering all energy components, that minimum-energy distance ought to be R = 3.5 Å with an offset of about 1.75 Å. Since induction is negligible, the difference is attributable to electrostatics. Indeed, E_{elst} affords contours that are attractive for $R \lesssim 3.75$ Å but largely ambivalent toward lateral displacement, at least for cofacial separations in the range 3.4 Å $\leq R \leq$ 3.8 Å (Figure 3c). For R = 3.4 Å, $E_{\mathrm{elst}} \approx -2$ kcal/mol and it is even more attractive at shorter separations. However, Pauli repulsion turns on quickly for $R < 3.4$ Å and limits further approach of the two arenes.

Short-range electrostatic stabilization thus plays an important role in establishing the minimum-energy value R = 3.4 Å for parallel-displaced π-stacking in benzene dimer, consistent with the conclusions of Cabaleiro-Lago et al.[23] This is also consistent with the pizza-π model that was suggested based on calculations for acene dimers up to $(\text{pentacene})_2$.[16] According to that model, electrostatic attraction (for $R < 3.8$ Å) provides the extra stabilization that is indicative of a specific π-stacking affect, differentiable from "normal" dispersion. That attractive interaction is not available in perpendicular edge-to-face geometries, where the electron-deficient hydrogen atoms prevent the onset of electrostatic attraction at close-contact distances.

3.2. Substituent and Heteroatom Modifications.

We next consider a variety of aromatic dimers in order to examine whether offset-stacking is controllable by tuning the balance of intermolecular forces, a frequent consideration in organic synthesis.[56,63] Polar substituents engender much larger electrostatic interactions as compared to benzene dimer, though we also consider $-CH_3$ as a nonpolar substituent. The toluene dimer has been suggested as a model of π−π interactions in proteins.[170]

3.2.1. Homomolecular Dimers.

We first consider $(C_6H_5X)_2$ for X = CH_3, OH, and CN. One-dimensional energy profiles for all three dimers are plotted in Figure 4, using the same lateral displacement coordinate that was examined for the benzene dimer. For each system, the face-to-face separation is set to that of the minimum-energy parallel-displaced geometry (R = 3.4−3.5 Å). These distances were obtained via potential energy scans with rigid monomer geometries, constrained so that the arenes remain coplanar, as described in Section S1.4.

Despite profound differences in the polarity of the substituents, each of these three dimers exhibits offset π-stacking with only minor variations, as judged by the similarities between E_{int} profiles in Figure 4. Induction energies are negligible and will not be considered further. For the toluene dimer (Figure 4a), electrostatic interactions are most favorable when the two arene moieties are in a sandwich arrangement with zero offset, analogous to the benzene dimer at a similar face-to-face separation (*cf.* Figure 2a). The vdW potential is repulsive at zero displacement but it does afford an offset on its own, albeit one that is slightly larger than the parallel-displacement that is observed when E_{elst} is added to the mix.

For the phenol and benzonitrile dimers, the polar substituents are arranged such that the dipole moment vectors of the two monomers are parallel to one another, as shown in the insets to Figure 4. In this arrangement, electrostatic interactions are nearly independent of the lateral displacement coordinate. Electrostatics is essentially negligible for $(\text{benzonitrile})_2$ but contributes a constant stabilization of −1.5 kcal/mol for $(\text{phenol})_2$. In either case, both E_{vdW} (on its own) and E_{int} (considering all energy components) predict similar offsets. This is remarkable similarity given that one of the substituents is electron-donating (Hammett parameter $\sigma_p = -0.37$ for OH) while the other is withdrawing ($\sigma_p = +0.66$ for CN).[171] The observed behavior is opposite to the prediction of the Hunter-Sanders rules,[64] insofar as an electron-withdrawing substituent would be inferred to reduce the quadrupole moment of the aromatic moiety, and thus reduce quadrupolar repulsion. In reality, $E_{\mathrm{elst}} < 0$ for $(\text{phenol})_2$ whereas $E_{\mathrm{elst}} \approx 0$ for for the benzonitrile dimer.

3.2.2. Heterocycles.

Biochemical π-stacking often involves heterocycles ranging from purines and pyrimidines in DNA to histidine and tryptophan in proteins. Previous calculations indicate that $(\text{pyridine})_2$ and the (pyridine)⋯(benzene) dimer display an even stronger preference for parallel-displaced stacking as compared to $(\text{benzene})_2$.[172,173] We next examine dimers of pyridine and thiophene as representative heterocycles, where the latter is a typical constituent of organic electronics.[174] Both monomers have a dipole moment (μ = 2.2

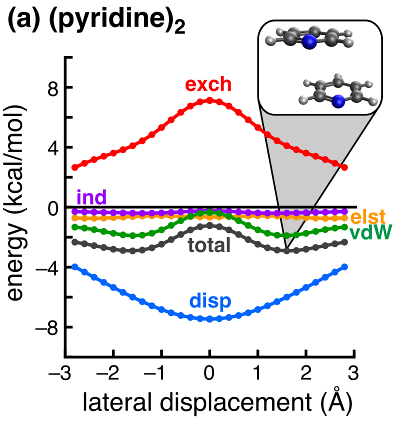

Figure 5. Energy component profiles for lateral slip-stacking in (a) (pyridine)$_2$ at R = 3.5 Å and (b) (thiophene)$_2$ at R = 3.6 Å. Face-to-face separations represent parallel-displaced minimum-energy values. Monomer dipole moments are aligned in parallel and lateral displacements are in the direction perpendicular to the monomer dipole axis.

D for pyridine and μ = 0.5 D for thiophene), so these systems might be anticipated to exhibit enhanced electrostatic interactions even in the absence of substituents. In fact, E_{elst} remains small. One-dimensional energy component profiles for (pyridine)$_2$ and (thiophene)$_2$ are plotted in Figure 5, using their minimum-energy parallel-displaced separations of 3.5 and 3.6 Å, respectively.

The situation for (pyridine)$_2$ largely parallels that of $(C_6H_5CN)_2$ at the same separation, insofar as E_{elst} is small and effectively independent of the lateral displacement (Figure 5a). As such, E_{vdW} parallels E_{int} with only a modest difference between the two, arising from the polarized electrostatics E_{elst}+ E_{ind}. Energy components for (thiophene)$_2$ are similar to those in (toluene)$_2$, with E_{elst} at its most attractive in the sandwich configuration (Figure 5b). For (thiophene)$_2$, the contribution from electrostatics is needed to obtain a bound potential because $E_{\text{vdW}} > 0$ when the lateral displacement is zero. Nevertheless, emergence of an offset-stacking double-well potential is driven by E_{vdW}. As in the benzene dimer, this means that short-range forces (dispersion and Pauli repulsion) are sufficient to furnish an offset.

Figure 6 plots two-dimensional lateral displacement profiles for (pyridine)$_2$ at two different face-to-face separations that bracket the value R = 3.5 Å that is used in Figure 5a. At both larger and smaller values of R, slip-stacking behavior is evident in the form of energy lowering for displacement in any lateral direction (Figure 6a,d), although the deepest wells correspond to displacements perpendicular to the monomer dipole axis. At R = 3.9 Å, these wells are clearly evident in E_{vdW} (Figure 6e), whereas E_{elst} is strictly repulsive and cannot explain offset stacking (Figure 6f). At R = 3.4 Å, a double-well structure remains in E_{vdW}, for displacement in any lateral direction (Figure 6b), but the sign of E_{elst} has switched from repulsive to attractive. At R = 3.4 Å, electrostatic attraction serves to deepen the wells very slightly.

3.2.3. Face-to-Face Distance Dependence.

For the cofacial benzene dimer, E_{elst} changes sign as one moves from the D_{6h} saddle point at R = 3.8 Å to the parallel-displaced geometry R = 3.4 Å. To explore this possibility in a wider variety of systems, we next consider one-dimensional lateral displacement potentials for dimers of aromatic heterocycles at different values of R.

Thiophene dimer exhibits similar face-to-face separation as benzene dimer, namely, R = 3.9 Å for the sandwich geometry and R = 3.5 Å for the parallel-displaced minimum (Table S1). Energy profiles at R = 3.4, 3.9, and 4.3 Å are shown in Figure 7, including all of the energy components discussed above along with $E_{\text{elst}} + E_{\text{exch}}$. As discussed elsewhere,[17] some DFT-based energy decomposition analyses compute electrostatic interactions using an antisymmetrized reference state, whereas SAPT-based methods do not. To compare the two, the antisymmetrized version of E_{elst} should be compared to SAPT-based $E_{\text{elst}} + E_{\text{exch}}$, which is provided here as a convenience.

For the chemist who might be tempted to conflate electron−electron Coulomb repulsion with Pauli (meaning steric) repulsion, the sum $E_{\text{elst}} + E_{\text{exch}}$ contains both. Note that steric repulsion originates in the Pauli Principle and its antisymmetry requirement, and is unrelated to electron−electron repulsion.[18] Pauli or exchange repulsion (E_{exch}) can be understood as the penalty to deform the monomer molecular orbitals in order to orthogonalize them with respect to an interacting partner, so that the orbitals of the dimer can be inserted into a single Slater determinant to satisfy the antisymmetry requirement.[18,175]

Considering thiophene dimer at R = 4.3 Å (Figure 7a), E_{elst} is repulsive across the entire range of lateral displacements, whereas for R = 3.4 Å the electrostatic interactions are strictly attractive (Figure 7c). At the intermediate value R = 3.9 Å, $E_{\text{elst}} \approx 0$ across the whole range of lateral displacements (Figure 7b). We consider each case in turn.

Atomic radii for two sulfur atoms sum to ≈3.6 Å,[165] so at R = 4.3 Å the monomers are well separated and there should be little charge penetration. In this case, E_{elst} is repulsive across the range of lateral displacements, consistent with dipolar and quadrupolar repulsion. Although the total electrostatic interaction does not exceed 0.5 kcal/mol at this separation, it is almost as repulsive as E_{exch}, whose magnitude falls off rapidly with distance and is much diminished at R = 4.3 Å, as compared to its value at smaller values of R. Nevertheless, the slip-stacked configuration is lower in energy as compared to the sandwich configuration, even at R = 4.3 Å. The shallow double minimum eliciting that behavior is present in E_{vdW}, which is also shallow to the point of being nearly flat in the region of ±1.8 Å displacement from the cofacial saddle point. The shallow double-minimum in E_{int} arises once one considers that electrostatics is slightly more repulsive at the zero-displacement saddle point, as compared to offset-stacked geometries.

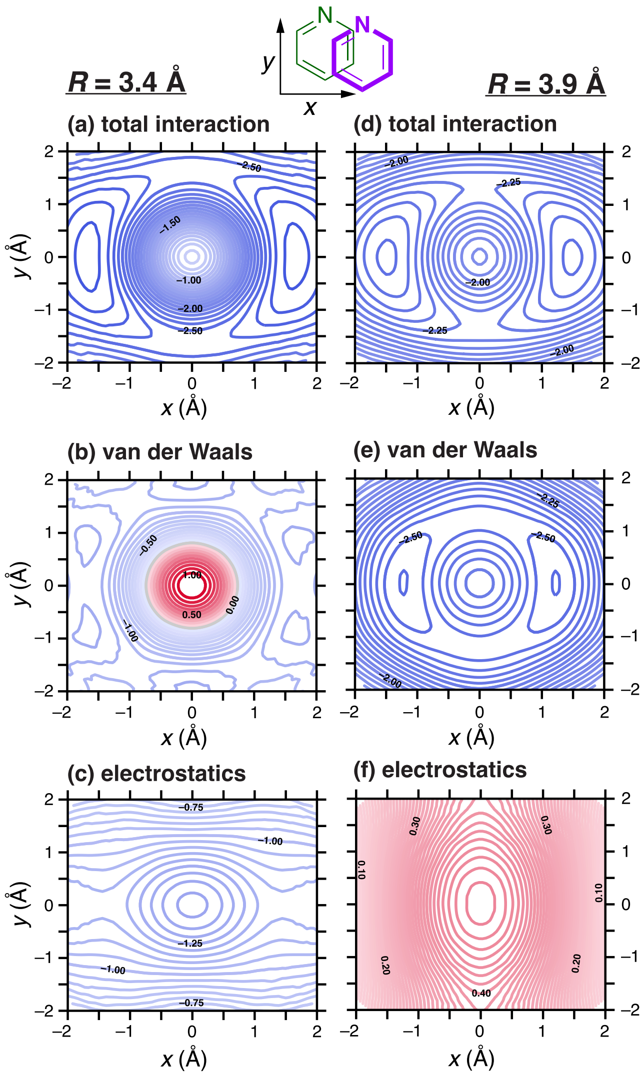

Figure 6. Energy component profiles for (pyridine)$_2$ at two different face-to-face separations: (a)−(c) R = 3.4 Å and (d)−(f) R = 3.9 Å. The origin represents the sandwich configuration and displacement directions are defined at the top. Red and blue contours indicate positive and negative energies, respectively, and selected contour values are labeled. For (a, b), contours are drawn every 0.1 kcal/mol and labeled every 0.5 kcal/mol. For (c)−(e), contours are given every 0.05 kcal/mol and labeled at intervals of 0.25 kcal/mol. For (f) the contours appear every 0.01 kcal/mol and are labeled every 0.1 kcal/mol.

At R = 3.9 Å both $|E_{\mathrm{elst}}|$ and $|E_{\mathrm{ind}}|$ are smaller than 0.2 kcal/mol so $E_{\mathrm{int}} \approx E_{\mathrm{vdW}}$ (Figure 7b). However, electrostatics switches from repulsive to attractive at smaller values of R, where the face-to-face separation is smaller than the sum of two sulfur atomic radii and charge penetration is significant. Note also that the maximum value of $|E_{\mathrm{elst}}|$ always coincides with the zero-offset sandwich geometry, regardless of whether electrostatics is attractive or repulsive.

For R = 3.4 Å, $E_{\mathrm{vdW}} > 0$ except at very large lateral displacements (Figure 7c). As such, the vdW potential alone would tend to dissociate the complex along the slip-stacking coordinate and electrostatics is necessary in order to stabilize the structure so that $E_{\mathrm{int}} < 0$. Given that E_{elst} is most attractive in the sandwich configuration, however, one must invoke E_{vdW} to explain offset-stacking.

A more nuanced picture emerges for the dimer of 1,3,5-triazine (also known as *s*-triazine), for which one-dimensional potentials are plotted in Figure 8 at the same values of R that were considered for (thiophene)$_2$. The total interaction potential exhibits a slip-stacked double minimum at each face-to-face separation but E_{vdW} exhibits only a single minimum (at the zero-offset sandwich configuration) for $R \gtrsim 3.9$ Å. For these larger separations, the double minimum emerges from E_{elst} rather than E_{vdW}.

If one *s*-triazine monomer is rotated by 180° at R = 3.4 Å then E_{elst} becomes more (and strictly) attractive, as shown in Figure 9. In this case, E_{int} exhibits only a single minimum at zero lateral displacement. The vdW potential is essentially unaffected by this 180° rotation, however, and maintains its double-well structure. It competes with E_{elst}, which has its minimum in the sandwich configuration, as it did also in (thiophene)$_2$. In the present case, that competition leads to a total interaction potential that is effectively flat for lateral displacements up to ±1 Å. Furthermore, electrostatics is responsible for the 3-fold-symmetric potential when one *s*-triazine monomer is rotated with respect to the other, along their mutual C_3 axis in the cofacial sandwich configuration; see Figure S2. Energy components E_{exch}, E_{ind}, and E_{disp} are entirely indifferent to the rotation angle and the variation is driven entirely by electrostatics. In the next section, we consider polar substituents and will find that $E_{\mathrm{exch}} + E_{\mathrm{disp}} + E_{\mathrm{ind}}$ remains indifferent with respect to the orientation of those substituents, whereas E_{elst} depends strongly on orientation.

3.3. Modulation by Electrostatics.

Results for aromatic heterocycles suggest that electrostatics can compete with vdW interactions to modulate the overall interaction energy profile in important ways. To examine this interdependence in detail, we next consider two-dimensional potentials for a variety of dimers, using both the face-to-face separation coordinate and the lateral displacement coordinate, analogous to the plots for benzene dimer in Figure 3.

3.3.1. Nitrobenzene Dimer.

In the $(C_6H_5X)_2$ examples considered in Section 3.2, substituent dipole moments were aligned in parallel. Here, we consider $(C_6H_5NO_2)_2$ in two orientations: one where the NO_2 substituents are arranged on the same end of the aromatic ring, so that their dipole moment vectors are parallel-aligned (Figure 10a−c), and another in which one monomer is rotated by 180° so that the dipole moment vectors are antiparallel (Figure 10d−f). In the first case, the potential is symmetric about zero for lateral displacements that align with the dipolar axis of the monomer, which is the horizontal coordinate in Figure 10. When the substituents are on opposite ends of the aromatic rings, the potential is highly asymmetric.

We consider the dipole-aligned orientation first. In this case, the symmetric double well in E_{int} has a clear antecedent in E_{vdW}, with a similar (though not identical) well depth and offset. At face-to-face separations $R \lesssim 3.5$ Å, the electrostatic component is attractive, serving to deepen the well, but it is largely ambivalent to lateral displacements (Figure 10c). For larger separations E_{elst} is repulsive, more so at zero displacement where the aromatic moieties assume a sandwich orientation. For this configuration, a case can be made that offset-stacking is driven by E_{vdW} although it is important to note that the face-to-face separation that would emerge from E_{vdW} alone is much larger ($R \approx 3.8$ Å) than what is observed on the full potential ($R \approx 3.45$ Å). It is the attractive contours of E_{elst} at short range that drive this reduction in R. Even so,

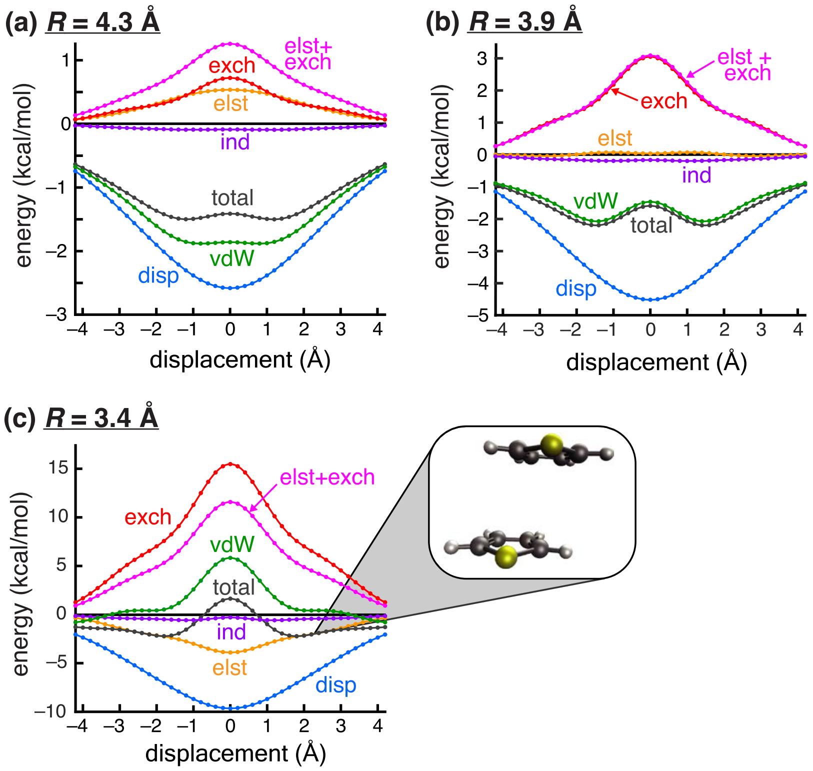

Figure 7. Energy components for $(\text{thiophene})_2$ at different face-to-face separations: (a) $R = 4.3$ Å, (b) $R = 3.9$ Å, and (c) $R = 3.4$ Å. The orientation of the monomers is shown in the inset and is the same at each value of R. Lateral displacements are perpendicular to the dipole axis of the monomer.

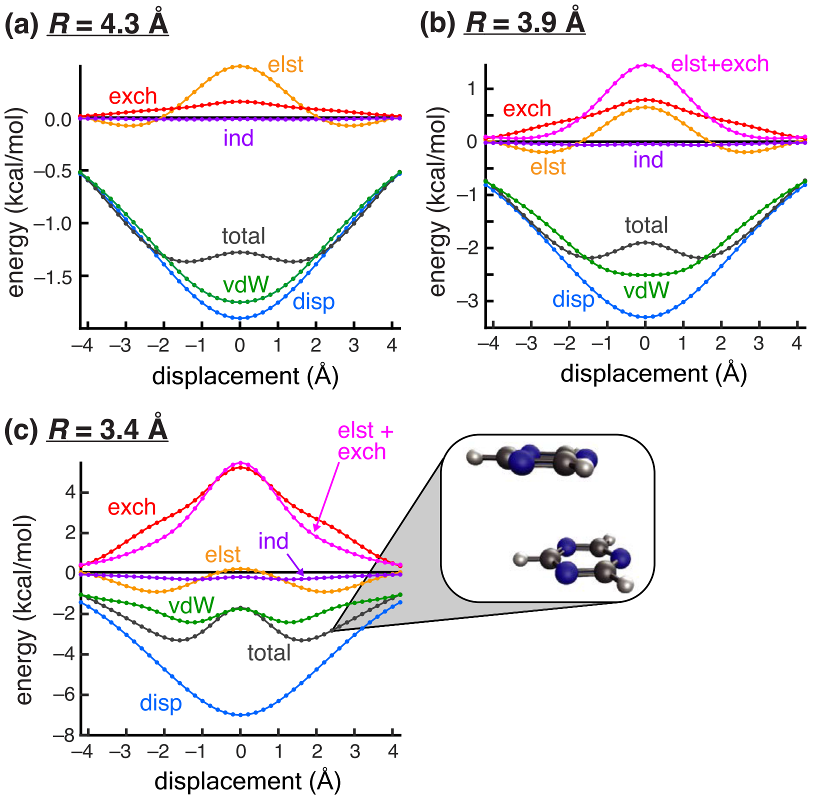

Figure 8. Energy component profiles for (s-triazine)$_2$ at various face-to-face separations: (a) $R = 4.3$ Å, (b) $R = 3.9$ Å, and (c) $R = 3.4$ Å. Monomers are arranged as shown in the inset.

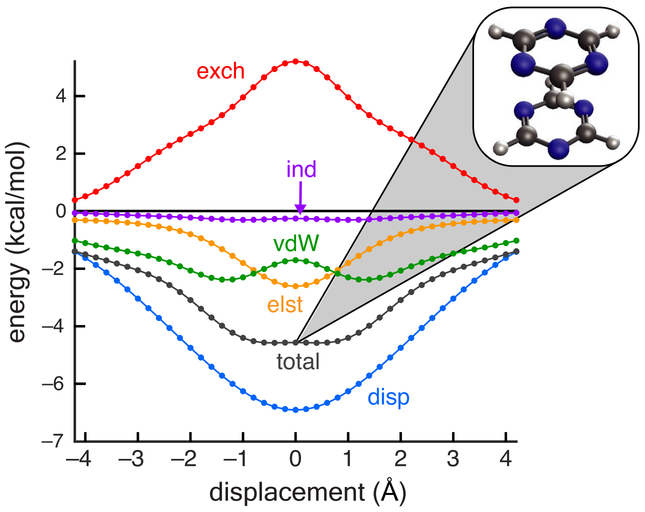

Figure 9. Energy component profiles for lateral displacements in (*s*-triazine)$_2$ at R = 3.4 Å. Relative to the data in Figure 8c, one monomer has been rotated by 180° with respect to the other.

this runs counter to a dipolar or quadrupolar electrostatics model.

Rotating one nitrobenzene monomer by 180° creates significant asymmetry in the potential, for displacements that align with the dipolar axis. The vdW potential predicts a lateral displacement of about the right magnitude (≈ 1.5 Å, see Figure 10e), but the vdW well depth is too shallow by about 3.75 kcal/mol and appears at too large a value of R. These discrepancies have clear origins in a very strong electrostatic driving force to place one NO_2 substituent directly atop the opposite aromatic ring, as evident in Figure 10f. This electrostatic effect can be imagined to "pull down" the vdW well to the smaller value of R where the minimum on the E_{int} surface is found, and in fact the same can be said for the parallel-dipole arrangement of $(C_6H_5NO_2)_2$. Thus, E_{elst} has a significant effect on tuning the lateral displacement potential.

3.3.2. *Pyrimidine Dimer.*

Stacking interactions in this system are qualitatively similar in several ways to those in the nitrobenzene dimer, and Figure 11 presents a two-dimensional scan that is analogous to the one we considered for that system. As with the nitrobenzene dimer, the parallel arrangement of the monomer dipoles (in Figure 11a−c) affords potentials that are symmetric about zero, for lateral displacements along the dipolar axis. A symmetric double-well structure of this sort exists already in E_{vdW} but at a too-large value of R. The remedy, as in the nitrobenzene dimer, lies in short-range electrostatic attraction that is mostly independent of lateral displacement (see Figure 11c). This situation closely mirrors that of the dipole-aligned nitrobenzene dimer.

For the antiparallel-dipole configuration (Figure 11e−f), the potential for lateral displacements is very asymmetric. Nevertheless, the situation is somewhat similar to the antiparallel arrangement of two nitrobenzene molecules except that in (pyrimidine)$_2$ the potential has developed a proper double-minimum, due to a deeper attractive well in E_{vdW}. The electrostatic driving force is somewhat asymmetric but does not favor nearly so large an offset as it did in $(C_6H_5NO_2)_2$, for which the polar bonds lie outside of the arene framework and that incentivizes a relatively large lateral displacement. In the antiparallel configuration of (pyrimidine)$_2$, the displacement is smaller and more consistent with that arising from E_{vdW}.

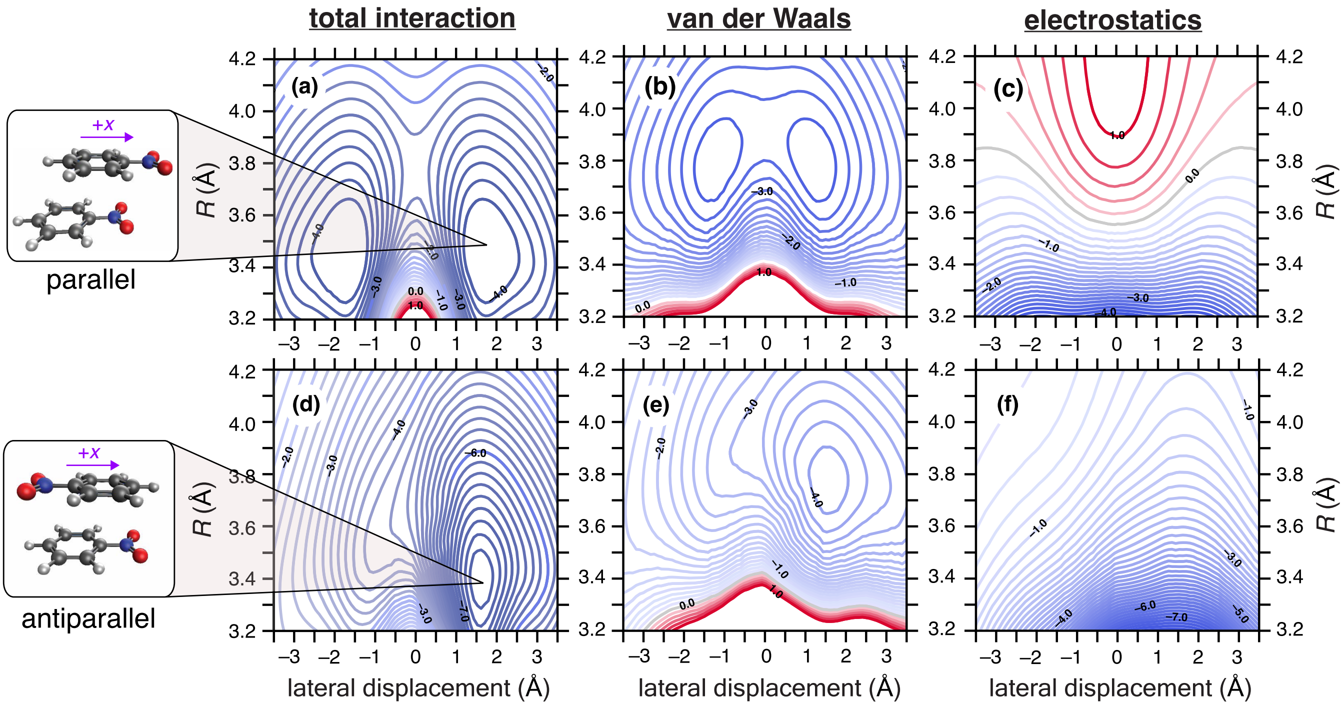

Figure 10. Potential energy scans for $(C_6H_5NO_2)_2$ in configurations where the monomer dipole moments are either (a)−(c) parallel-aligned or else (d)−(f) in an antiparallel configuration, as shown in the insets at left. The vertical coordinate is the cofacial separation R and the horizontal coordinate represents lateral displacement along the dipolar axis (as shown in the insets), leading to potentials that are symmetric about zero in (a)−(c). Contours are drawn every 0.2 kcal/mol and labeled every 1.0 kcal/mol, with blue and red indicating negative and positive energy values, respectively.

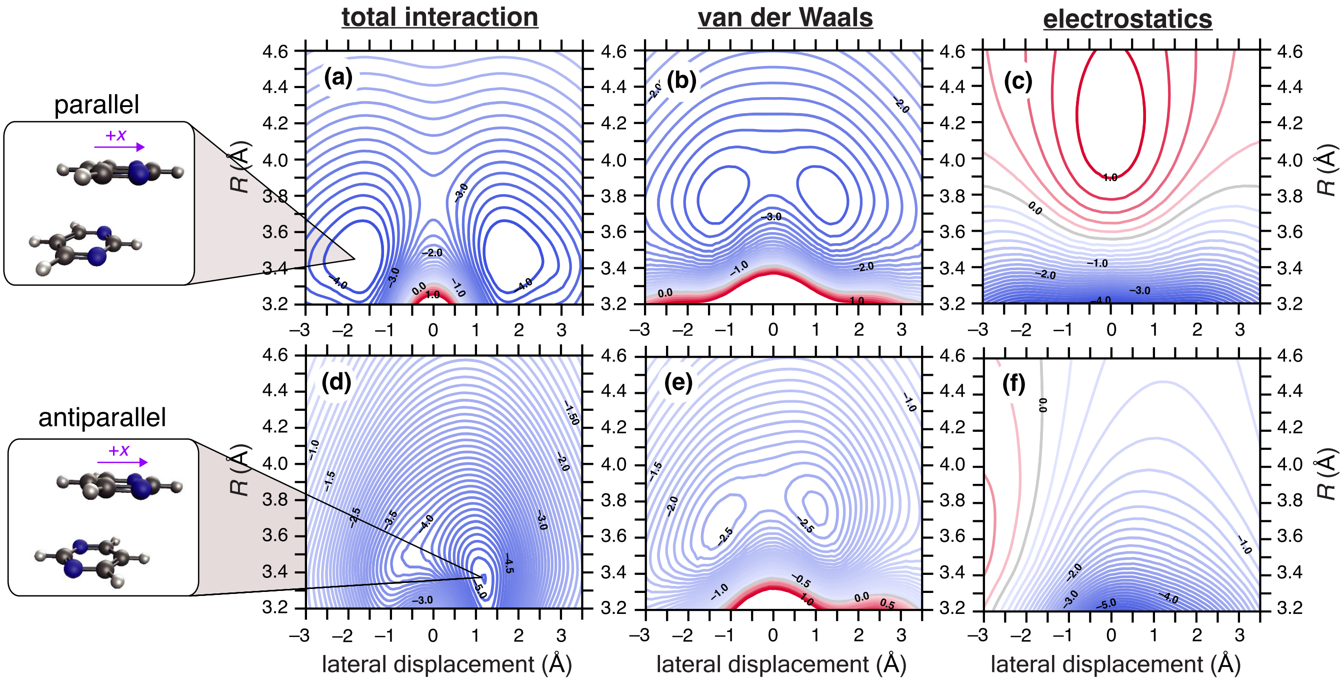

Figure 11. Energy component profiles for $(\text{pyrimidine})_2$ with (a)−(c) parallel or (d)−(f) antiparallel monomer dipole moments. Lateral displacements are parallel to the dipolar axis, in the direction indicated in the insets at left. Contours are drawn every 0.1 kcal/mol and labeled every 0.5 kcal/mol, with blue and red indicating negative and positive energies, respectively.

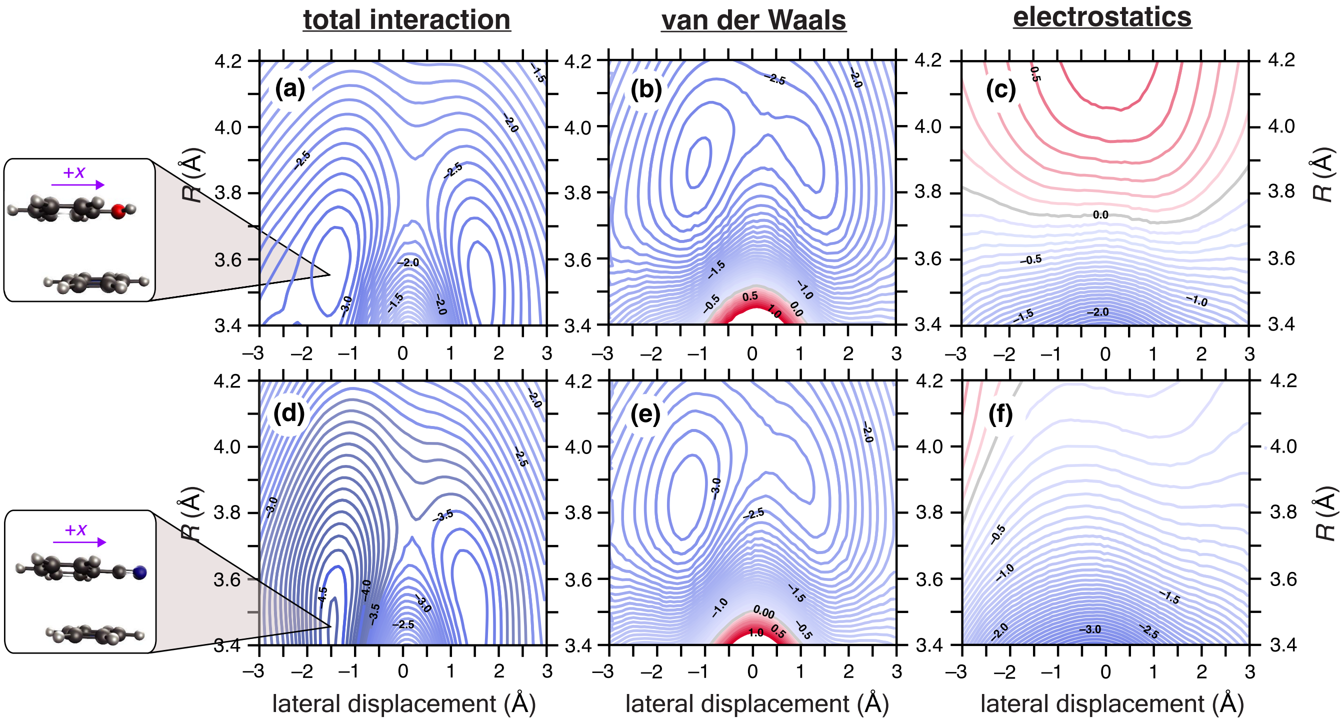

Figure 12. Two-dimensional energy component profiles as a function of the face-to-face separation and a lateral displacement coordinate, for (a)−(c) benzene atop phenol versus (d)−(f) benzene on benzonitrile. The lateral coordinate coincides with the C−X axis of the C_6H_5X monomer, with the + x direction indicated in the insets at left. Contours are drawn every 0.1 kcal/mol and labeled every 0.5 kcal/mol, with blue and red indicating negative and positive energies, respectively.

3.3.3. $(C_6H_6)\cdots(C_6H_5X)$. Benzene dimers with a single substituent allow us to isolate the polar substituent's contributions to the energetics in the absence of a dipole moment on the opposite monomer. Previous theoretical work has established the existence of parallel-displaced minima in systems such as $(C_6H_6)\cdots(C_6H_5NO_2)$,[176] with electrostatics as a weaker interaction as compared to dispersion. Two-dimensional energy profiles for $(C_6H_6)\cdots(C_6H_5X)$, with X = OH or CN, are plotted in Figure 12.

Examining these two dimers in the context of the polar, homomolecular dimers considered above, a throughline emerges. On its own, E_{vdW} provides sufficient driving force

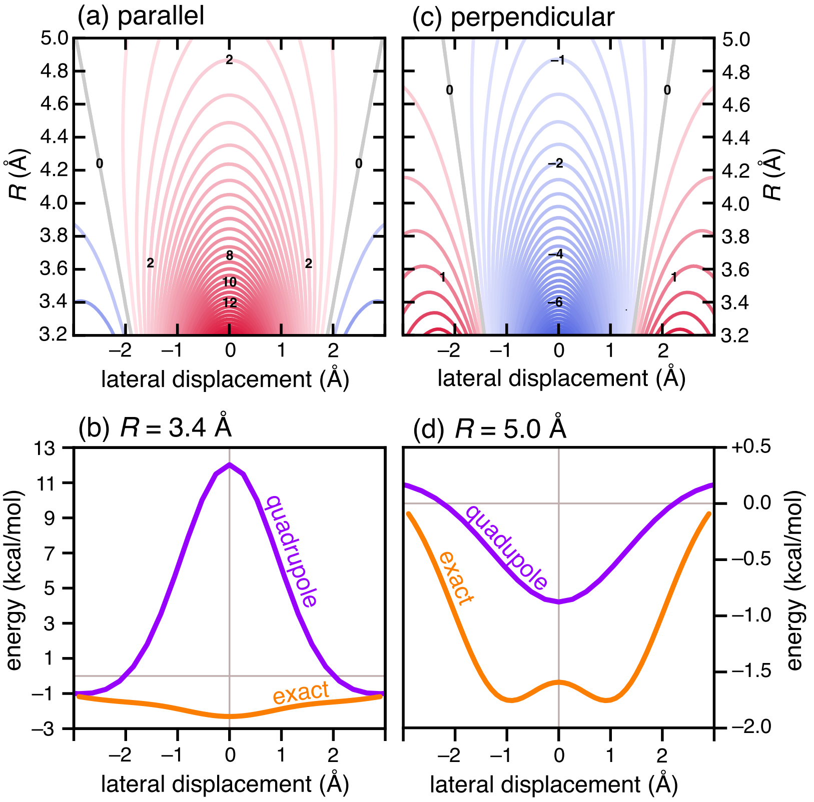

Figure 13. Electrostatic interaction potentials for $(C_6H_6)_2$. (a) Two-dimensional contours of the quadrupole−quadrupole interaction for a coplanar arrangement, with the sandwich structure at zero displacement, computed using a quadrupole moment that is consistent with XSAPT + MBD electrostatics. Contours are drawn in 0.5 kcal/mol intervals. For comparison, the analogous electrostatic potential computed using full charge densities can be found in Figure 3. (b) One-dimensional slice for coplanar $(C_6H_6)_2$ at $R = 3.4$ Å, comparing the quadrupolar result from (a) to an exact calculation of E_{elst} using eq 2. (c) Contours of the quadrupole−quadrupole interaction for a perpendicular configuration of $(C_6H_6)_2$, with the T-shaped geometry at zero displacement. Contours appear at 0.25 kcal/mol intervals. (d) One-dimensional potential at a 5.0 Å center-to-center distance (consistent with the T-shaped saddle point), comparing the quadrupolar interaction potential from (c) with an exact calculation of E_{elst}. In (a, c), both distance scales are the same but the energy scales differ between (b, d).

for a lateral offset, which may or may not be symmetric depending on the nature of the substituents, but which appears at a face-to-face separation that is significantly larger than that of the true minimum-energy value. Short-range electrostatics, which is attractive but does not depend strongly on the lateral displacement, is needed to bring R into alignment with the value obtained from the total interaction potential. This description fits the $(C_6H_6)\cdots(C_6H_5OH)$ and $(C_6H_6)\cdots(C_6H_5CN)$ systems as well as the nitrobenzene and pyrimidine dimers.

3.4. Failure of Quadrupolar Electrostatics. Results above demonstrate that the slip-stacking phenomenon (meaning the existence of a lateral offset) can be explained in many cases by competition between dispersion and Pauli repulsion, with the latter favoring the cofacial sandwich that maximally places atoms and π electron density into close proximity, whereas E_{exch} is reduced by moving the two arenes farther apart. This competition is codified into E_{vdW}. However, results in Section 3.3 clearly demonstrate that E_{vdW} cannot capture the strong asymmetry of the potential energy surface for polar substituents or polar heterocycles, because it is typically insensitive (or only moderately sensitive) to the relative orientation of the two monomers. Capturing the asymmetry requires consideration of electrostatic interactions that depend strongly on the relative orientation of polar substituents or (in the case of unsubstituted heterocycles such as pyrimidine) the relative orientation of the monomer dipole moments.

That said, an equally consistent theme is that short-range electrostatic interactions are typically attractive for cofacial arenes, notwithstanding any considerations based on the monomer dipole and/or quadrupole moments. In that sense, the picture that emerges from detailed calculations is very different from the conventional view of π-stacking.[30,35] To emphasize this, we next examine approximate electrostatic potentials computed using only the dipole and quadrupole moments for the monomers. These results are qualitatively different from exact electrostatics, in misleading ways. Details of the multipolar electrostatics calculations can be found in Section S1.2.2. Here, it suffices to say that the monomer dipole moment vectors and quadrupole moment tensors were computed at the LRC-ωPBE/def2-TZVPD level,[177] consistent with the description of the monomers in the XSAPT + MBD calculations (see Section S1.3).

We begin with parallel and perpendicular arrangements of $(C_6H_6)_2$. Figure 13a shows a two-dimensional scan of the quadrupole−quadrupole interaction potential for two cofacial benzene monomers, which should be compared to the corresponding plot of the exact electrostatic interaction energy (E_{elst}) in Figure 3c. The two plots are qualitatively different. The exact electrostatic interaction is attractive for $R < 3.7$ Å,[18,34] but is mostly ambivalent with regard to small lateral displacements. In fact, it exhibits a shallow minimum at zero lateral displacement, as seen in the one-dimensional cut (for $R = 3.4$ Å) that is shown in Figure 13b. In contrast, the

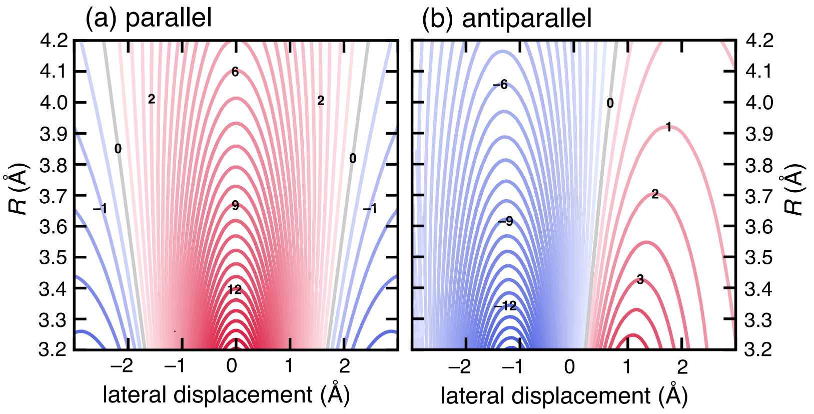

Figure 14. Approximate electrostatic potentials for cofacial $(C_6H_5NO_2)_2$ in orientations where the monomer dipole moments are either (a) parallel or (b) antiparallel. In either case, the electrostatic potential is approximated using monomer dipole and quadrupole moments computed at a level of theory that is consistent with XSAPT+MBD electrostatics. Contours are plotted every 0.5 kcal/mol. Exact results using full charge densities (eq 2) can be found in Figure 10c,10f for the parallel and antiparallel configurations, respectively.

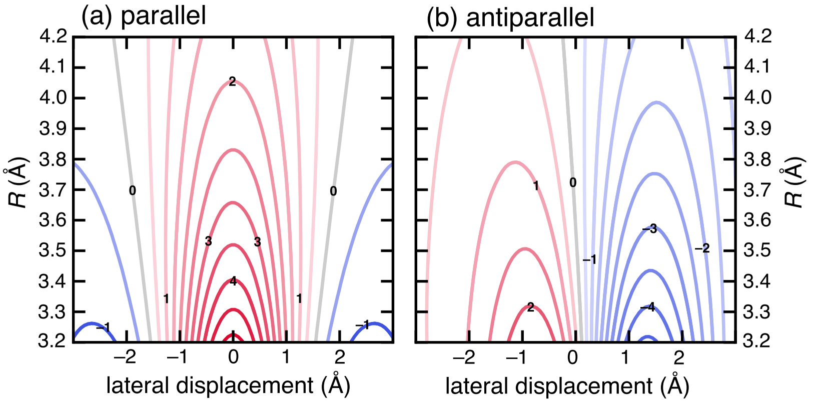

Figure 15. Approximate electrostatic potentials for cofacial (pyrimidine)$_2$ in orientations where the monomer dipole moments are either (a) parallel or (b) antiparallel. In either case, the electrostatic potential is approximated using monomer dipole and quadrupole moments computed at a level of theory that is consistent with XSAPT+MBD electrostatics. Contours are plotted every 0.5 kcal/mol. Exact results using full charge densities can be found in Figure 11c,f for the parallel and antiparallel configurations, respectively.

quadrupole−quadrupole interaction is extremely repulsive in the sandwich geometry and decays much more rapidly along the lateral displacement coordinate.

Although our focus in this work has been on cofacial offset-stacking, it bears pointing out that the quadrupolar description of electrostatics is also qualitatively wrong in edge-to-face geometries. For the perpendicular arrangement of $(C_6H_6)_2$, exact electrostatics favors an L-shaped configuration with a small offset of about 1.1 Å, as discussed in previous work.[17] This is readily apparent in the one-dimensional cuts that are provided in Figure 13d for $R = 5.0$ Å, which is the center-to-center distance of the two benzene rings in the T-shaped saddle point. The quadrupole−quadrupole potential is also attractive near the T-shaped minimum but favors the T-shaped (C_{2v}) geometry rather than an L-shaped one.

For examples where polar substituents lend asymmetry to E_{elst}, we consider $(C_6H_5NO_2)_2$ in Figure 14 and (pyrimidine)$_2$ in Figure 15. In both cases, what is plotted are contours of the electrostatic interaction surface obtained when only the monomer dipole and quadrupole moments are considered. As in previous calculations for these two systems, the monomers are in a coplanar arrangement and we consider both parallel and antiparallel alignments of the monomer dipole moment vectors. Lateral displacements are taken parallel to the dipolar axis of the monomers. This way, results for $(C_6H_5NO_2)_2$ in Figure 14 can be compared to exact electrostatics calculations in Figure 10c,f, and results for (pyrimidine)$_2$ in Figure 15 can be compared to exact results in Figure 11c,f.

When the monomer dipole moments are parallel-aligned, the multipolar electrostatics results are qualitatively similar in $(C_6H_5NO_2)_2$ and (pyrimidine)$_2$, even if the interactions are much stronger for the former. These dipole-aligned multipolar potentials are also qualitatively similar to the quadrupole−quadrupole interactions in benzene dimer (Figure 13a), in the sense that the sandwich configuration is strongly repulsive and there are shallow wells for lateral displacement (slip-stacking). Setting aside the magnitude of these offsets, this is qualitatively wrong behavior for electrostatics, as demonstrated by comparison to exact results. In the exact calculation (in Figure 10c for the nitrobenzene dimer and in Figure 11c for the pyrimidine dimer), $E_{\text{elst}} < 0$ at short range but the contours are largely ambivalent to lateral displacement. This is similar to the situation in benzene dimer and indicates that the dipole + quadrupole approximation fails for these polar systems, in the same way that quadrupolar electrostatics fails for $(C_6H_6)_2$.

For the antiparallel-aligned geometries of the nitrobenzene and pyrimidine dimers, the multipolar calculation provides a strong driving force for lateral displacement, e.g., in a direction that places one NO_2 substituent atop the opposite arene in

$(C_6H_5NO_2)_2$. (The driving force lies in the opposite direction for the pyrimidine dimer due to differences in the dipole–quadrupole interactions.) Multipolar interactions are thus strongly asymmetric with respect to lateral displacements, but in a manner that is inconsistent with exact electrostatics. For the latter, Figures 10f and 11f show that E_{elst} exhibits only mild asymmetry for lateral displacement. The exact result is generally attractive for $R \lesssim 3.8$ Å, at least for any lateral displacement consistent with π-stacking. This is altogether different from the multipolar result that exhibits both strongly attractive but also strongly repulsive regions for the same value of R, depending on the lateral displacement.

4. CONCLUSIONS

There is no basis for continued invocation of quadrupolar electrostatics, or electron–electron repulsion at all, in order to explain offset π-stacking between nonpolar arene moieties. The quadrupolar picture, which has been characterized as "neat, simple, and wrong",[18] does not account for the fact that charge penetration is significant at typical nonbonded close-contact distances, including π-stacking distances (3.4–3.8 Å face-to-face separation). As a result, electrostatic interactions may differ in sign with respect to what would be inferred from the leading-order molecular multipole moments, or even from distributed multipoles.[20,31,34] Very often, electrostatic interactions are attractive in face-to-face π-stacked geometries,[16−18,20,31,34] as the gain in intermolecular electron–nucleus attraction at short range compensates for additional electron–electron repulsion.[18] As such, the ubiquitous cartoon charge distributions in Figure 1 are misleading and perhaps ought to be retired.

In view of this, an alternative explanation for offset π-stacking is required. Using a diverse array of aromatic dimers, including substituted benzenes and heterocycles, we have demonstrated that electrostatic interactions are neither necessary nor sufficient to drive π-stacked systems into parallel-displaced geometries. Instead, this behavior is driven by the combination of dispersion and Pauli repulsion, i.e., by vdW interactions.[16−19] The preference for parallel-displaced π-stacking may be enhanced or opposed by electrostatics, but it emerges nonetheless. Meanwhile, approximate electrostatic interactions computed by considering only the monomer dipole and quadrupole moments bear little resemblance to exact electrostatic energies computed using the full change densities of the interacting monomers. At typical face-to-face π-stacking distances (3.4–3.8 Å), rigorous quantum-mechanical calculation of the Coulomb interaction between monomer charge densities, rather than any finite-order multipolar approximation, is necessary in order to safely draw conclusions about electrostatic interactions.

Competition between dispersion and Pauli repulsion provides a basis for offset-stacking that requires only short-range forces, rather than longer-ranged electrostatics. This explains the pervasive nature of parallel-displaced π-stacking between aromatic side chains in proteins,[24] and the near absence of cofacial π-stacking in those systems,[40] across myriad local electrostatic environments. The arene moieties bring the short-range forces with them wherever they go, regardless of what might be happening in terms of electrostatics. That said, E_{vdW} is largely unchanged by rotation of one cofacial arene with respect to its π-stacked partner. Therefore, in cases involving polar substituents or heterocycles, one must also consider E_{elst} in order to predict the relative orientation of the two arenes, and to correctly predict the preferred direction of the slip-stacking phenomenon.

A better understanding of the molecular physics underlying π–π interactions is important for rational design of supramolecular structures; our data present a clear roadmap for those looking to rationalize and utilize such interactions. Consideration of electron-donating or withdrawing effects within the context of the Hunter-Sanders rules[64] is not an effective guide.[10,20] Instead, one should look to the "direct interaction model" of Wheeler and Houk to explain substituent effects on stacking energies.[12,123−127] At the same time, our work suggests that substituent modifications alone may be insufficient to avoid offset-stacking in supramolecular frameworks and other soft materials.[21]

ASSOCIATED CONTENT

Supporting Information

The Supporting Information is available free of charge at https://pubs.acs.org/doi/10.1021/jacs.4c13291.

Additional one- and two-dimensional potential energy scans and details of the computational procedure (PDF)

Raw data for the energy components used to make the plots (XLSX)

Coordinates for all monomers considered (TXT)

AUTHOR INFORMATION

Corresponding Author

John M. Herbert – *Department of Chemistry and Biochemistry, The Ohio State University, Columbus, Ohio 43210, United States;* orcid.org/0000-0002-1663-2278; Email: herbert@chemistry.ohio-state.edu

Authors

Brandon Schramm – *Department of Chemistry and Biochemistry, The Ohio State University, Columbus, Ohio 43210, United States;* Present Address: Department of Chemistry, University of California, Berkeley, California 94720 USA

Montgomery Gray – *Department of Chemistry and Biochemistry, The Ohio State University, Columbus, Ohio 43210, United States*

Complete contact information is available at: https://pubs.acs.org/10.1021/jacs.4c13291

Author Contributions

†B.S. and M.G. contributed equally to this work

Notes

The authors declare the following competing financial interest(s): J.M.H. is part owner of Q-Chem Inc. and serves on its board of directors.

ACKNOWLEDGMENTS

Work by B.S. was supported by the National Science Foundation (CHE-1955282). Work by M.G. was supported by the National Institute of General Medical Sciences of the National Institutes of Health under Award No. 1R43GM148095-01A1, and by a Presidential Fellowship from the Ohio State University. Development of XSAPT was supported by the U.S. Department of Energy, Office of Basic Energy Sciences, Division of Chemical Sciences, Geosciences, and Biosciences under Award No. DE-SC0008550. Calculations were performed at the Ohio Supercomputer Center.[178]

REFERENCES

(1) McGaughey, G. B.; Gagné, M.; Rappé, A. K. π-stacking interactions: Alive and well in proteins. *J. Biol. Chem.* **1998**, *273*, 15458−15463.

(2) Hunter, C. A.; Lawson, K. R.; Perkins, J.; Urch, C. J. Aromatic interactions. *J. Chem. Soc., Perkin Trans. 2* **2001**, *2*, 651−669.

(3) Brandl, M.; Weiss, M. S.; Jabs, A.; Sühnel, J.; Hilgenfeld, R. C-H···π interactions in proteins. *J. Mol. Biol.* **2001**, *307*, 357−377.

(4) He, X.; Fusti-Molnar, L.; Cui, G.; Merz, K. M., Jr. The importance of dispersion and electron correlation in ab initio protein folding. *J. Phys. Chem. B* **2009**, *113*, 5290−5300.

(5) Pérez, E. M.; Martín, N. π−π interactions in carbon nanostructures. *Chem. Soc. Rev.* **2015**, *44*, 6425−6433.

(6) Maji, R.; Wheeler, S. E. Role of Aromatic Interactions in Directing Organic Reactions. In *Aromatic Interactions: Frontiers in Knowledge and Applications*; Johnson, D. W.; Hof, F., Eds.; Royal Society of Chemistry: Cambridge, 2017; Vol. *20*, Chapter 2, pp 18−38.

(7) Xu, Z.; Zhang, Q.; Shi, J.; Zhu, W. Underestimated noncovalent interactions in protein data bank. *J. Chem. Inf. Model.* **2019**, *59*, 3389−3399.

(8) Zhuang, W.-R.; Wang, Y.; Cui, P.-F.; Xing, L.; Lee, J.; Kim, D.; Jiang, H.-L.; Oh, Y.-K. Applications of π−π stacking interactions in the design of drug-delivery systems. *J. Controlled Release* **2019**, *294*, 311−326.

(9) Deng, J.-H.; Luo, J.; Mao, Y.-L.; Lai, S.; Gong, Y.-N.; Zhong, D.-C.; Lu, T.-B. π−π stacking interactions: Non-negligible forces for stabilizing porous supramolecular framework. *Sci. Adv.* **2020**, *6*, No. eaax9976.

(10) Sinnokrot, M. O.; Sherrill, C. D. Substituent effects in π−π interactions: Sandwich and T-shaped configurations. *J. Am. Chem. Soc.* **2004**, *126*, 7690−7697.

(11) Hohenstein, E. G.; Duan, J.; Sherrill, D. C. Origin of the surprising enhancement of electrostatic energies by electron-donating substituents in substituted sandwich benzene dimers. *J. Am. Chem. Soc.* **2011**, *133*, 13244−13247.

(12) Wheeler, S. E. Understanding substituent effects in noncovalent interactions involving aromatic rings. *Acc. Chem. Res.* **2013**, *46*, 1029−1038.

(13) Martinez, C. R.; Iverson, B. L. Rethinking the term "pi-stacking. *Chem. Sci.* **2012**, *3*, 2191−2201.

(14) Grimme, S. Do special noncovalent π−π stacking interactions really exist? *Angew. Chem., Int. Ed.* **2008**, *47*, 3430−3434.

(15) Ninković, D. B.; Filipović, J. P. B.; Hall, M. B.; Brothers, E. N.; Zarić, S. D. What is special about aromatic-aromatic interactions? Significant attraction at large horizontal displacement. *ACS Cent. Sci.* **2020**, *6*, 420−425.

(16) Carter-Fenk, K.; Herbert, J. M. Reinterpreting π-stacking. *Phys. Chem. Chem. Phys.* **2020**, *22*, 24870−24886.

(17) Carter-Fenk, K.; Herbert, J. M. Electrostatics does not dictate the slip-stacked arrangement of aromatic π−π interactions. *Chem. Sci.* **2020**, *11*, 6758−6765.

(18) Herbert, J. M. Neat, simple, and wrong: Debunking electrostatic fallacies regarding noncovalent interactions. *J. Phys. Chem. A* **2021**, *125*, 7125−7137.

(19) Carter-Fenk, K.; Lao, K. U.; Herbert, J. M. Predicting and understanding non-covalent interactions using novel forms of symmetry-adapted perturbation theory. *Acc. Chem. Res.* **2021**, *54*, 3679−3690.

(20) Sherrill, C. D. Energy component analysis of π interactions. *Acc. Chem. Res.* **2013**, *46*, 1020−1028.

(21) Gray, M.; Herbert, J. M. Origins of offset-stacking in porous frameworks. *J. Phys. Chem. C* **2023**, *127*, 2675−2686.

(22) Cabaleiro-Lago, E. M.; Rodríguez-Otero, J. σ-σ, σ-π, and π−π stacking interactions between six-membered cyclic systems. Dispersion dominates and electrostatics commands. *ChemistrySelect* **2017**, *2*, 5157−5166.

(23) Cabaleiro-Lago, E. M.; Rodríguez-Otero, J.; Vázquez, S. A. Electrostatic penetration effects stand at the heart of aromatic π interactions. *Phys. Chem. Chem. Phys.* **2022**, *24*, 8979−8991.

(24) Carter-Fenk, K.; Liu, M.; Pujal, L.; Loipersberger, M.; Tsanai, M.; Vernon, R. M.; Forman-Kay, J. D.; Head-Gordon, M.; Heidar-Zadeh, F.; Head-Gordon, T. The energetic origins of pi-pi contacts in proteins. *J. Am. Chem. Soc.* **2023**, *145*, 24836−24851.

(25) Corminboeuf, C.; von Ragué Schleyer, P.; Warner, P. Are antiaromatic rings stacked face-to-face aromatic? *Org. Lett.* **2007**, *9*, 3263−3266.

(26) Björk, J.; Hanke, F.; Palma, C.-A.; Samori, P.; Cecchini, M.; Persson, M. Adsorption of aromatic and anti-aromatic systems on graphene through π−π stacking. *J. Phys. Chem. Lett.* **2010**, *1*, 3407−3412.

(27) Bloom, J. W. G.; Wheeler, S. E. Taking the aromaticity out of aromatic interactions. *Angew. Chem., Int. Ed.* **2011**, *50*, 7847−7849.

(28) Vernon, R. M.; Chong, P. A.; Tsang, B.; Kim, T. H.; Bah, A.; Farber, P.; Lin, H.; Forman-Kay, J. D. Pi-pi contacts are an overlooked protein feature relevant to phase separation. *eLife* **2018**, *7*, No. e31486.

(29) Molčanov, K.; Milašinović, V.; Kojić-Prodić, B. Contribution of different crystal packing forces in π-stacking: From noncovalent to covalent multicentric bonding. *Cryst. Growth Des.* **2019**, *19*, 5967−5980.

(30) Molčanov, K.; Kojić-Prodić, B. Towards understanding π-stacking interactions between non-aromatic rings. *IUCrJ* **2019**, *6*, 156−166.

(31) Price, S. L.; Stone, A. J. The electrostatic interactions in van der Waals complexes involving aromatic molecules. *J. Chem. Phys.* **1987**, *86*, 2859−2868.

(32) Sinnokrot, M. O.; Sherrill, C. D. Highly accurate coupled cluster potential energy curves for the benzene dimer: Sandwich, T-shaped, and parallel-displaced configurations. *J. Phys. Chem. A* **2004**, *108*, 10200−10207.

(33) Podeszwa, R.; Bukowski, R.; Szalewicz, K. Potential energy surface for the benzene dimer and perturbational analysis of π−π interactions. *J. Phys. Chem. A* **2006**, *110*, 10345−10354.

(34) Ryno, S. M.; Risko, C.; Brédas, J.-L. Noncovalent interactions and impact of charge penetration effects in linear oligoacene dimers and single crystals. *Chem. Mater.* **2016**, *28*, 3990−4000.

(35) Fagnani, D. E.; Sotuyo, A.; Castellano, R. K. π−π Interactions. In *Comprehensive Supramolecular Chemistry II*; Elsevier: Oxford, 2017; Vol. *1*, Chapter 6, pp 121−148.

(36) Sinnokrot, M. O.; Valeev, E. F.; Sherrill, C. D. Estimates of the ab initio limit for π−π interactions: The benzene dimer. *J. Am. Chem. Soc.* **2002**, *124*, 10887−10893.

(37) Tsuzuki, S.; Honda, K.; Uchimaru, T.; Mikami, M. High-level ab initio computations of structures and interaction energies of naphthalene dimers: Origin of attraction and its directionality. *J. Chem. Phys.* **2004**, *120*, 647−659.

(38) Podeszwa, R.; Szalewicz, K. Physical origins of interactions in dimers of polycyclic aromatic hydrocarbons. *Phys. Chem. Chem. Phys.* **2008**, *10*, 2735−2746.

(39) Silva, N. J.; Machado, F. B. C.; Lischka, H.; Aquino, A. J. A. π−π stacking between polyaromatic hydrocarbon sheets beyond dispersion interactions. *Phys. Chem. Chem. Phys.* **2016**, *18*, 22300−22310.

(40) Hunter, C. A.; Singh, J.; Thornton, J. M. π−π interactions: The geometry and energetics of phenylalanine-phenylalanine interactions in proteins. *J. Mol. Biol.* **1991**, *218*, 837−846.

(41) Janiak, C. A critical account on π−π stacking in metal complexes with aromatic nitrogen-containing ligands. *J. Chem. Soc., Dalton Trans.* **2000**, 3885−3896.

(42) Banerjee, A.; Saha, A.; Saha, B. K. Understanding the behavior of π−π interactions in crystal structures in light of geometry corrected statistical analysis: Similarities and differences with the theoretical models. *Cryst. Growth Des.* **2019**, *19*, 2245−2252.

(43) Fleming, I. *Molecular Orbitals and Organic Chemical Reactions*; John Wiley & Sons: Chichester, United Kingdom, 2010.

(44) Zou, Y.; Hou, X.; Wei, H.; Shao, J.; Jiang, Q.; Ren, L.; Wu, J. Circumcoronenes. *Angew. Chem., Int. Ed.* **2023**, *62*, No. e202301041.

(45) Bayse, C. A. Stack bonding in polycyclic aromatic hydrocarbons. *Phys. Chem. Chem. Phys.* **2023**, *25*, 20451−20461.

(46) Zhang, Z.; Zhu, H.; Gu, J.; Shi, H.; Hirose, T.; Jiang, L.; Zhu, Y.; Zhong, D.; Wang, J. Nonplanar nanographene with a large conjugated π-surface. *J. Am. Chem. Soc.* **2024**, *146*, 24681−24688.

(47) Spitler, E. L.; Koo, B. T.; Novotney, J. L.; Colson, J. W.; Uribe-Romo, F. J.; Gutierrez, G. D.; Clancy, P.; Dichtel, W. R. A 2D covalent organic framework with 4.7-nm pores and insight into its interlayer stacking. *J. Am. Chem. Soc.* **2011**, *133*, 19416−19421.

(48) Lukose, B.; Kuc, A.; Heine, T. The structure of layered covalent-organic frameworks. *Chem. - Eur. J.* **2011**, *17*, 2388−2392.

(49) Koo, B. T.; Dichtel, W. R.; Clancy, P. A classification scheme for the stacking of two-dimensional boronate ester-linked covalent organic frameworks. *J. Mater. Chem.* **2012**, *22*, 17460−17469.

(50) Du, Y.; Calabro, D.; Wooler, B.; Li, Q.; Cundy, S.; Kamakoti, P.; Colmyer, D.; Mao, K.; Ravikovitch, P. Kinetic and mechanistic study of COF-1 phase change from a staggered to eclipsed model upon partial removal of mesitylene. *J. Phys. Chem. C* **2014**, *118*, 399−407.

(51) Haase, F.; Gottschling, K.; Stegbauer, L.; Germann, L. S.; Gutzler, R.; Duppel, V.; Vyas, V. S.; Kern, K.; Dinnebier, R. E.; Lotsch, B. V. Tuning the stacking behaviour of a 2D covalent organic framework through non-covalent interactions. *Mater. Chem. Front.* **2017**, *1*, 1354−1361.

(52) Wu, X.; Han, X.; Liu, Y.; Liu, Y.; Cui, Y. Control interlayer stacking and chemical stability of two-dimensional covalent organic frameworks via steric tuning. *J. Am. Chem. Soc.* **2018**, *140*, 16124−16133.

(53) Geng, K.; He, T.; Liu, R.; Dalapati, S.; Tan, K. T.; Li, Z.; Tao, S.; Gong, Y.; Jiang, Q.; Jiang, D. Covalent organic frameworks: Design, synthesis, and functions. *Chem. Rev.* **2020**, *120*, 8814−8933.

(54) Bishop, R. New Aspects of Aromatic π···π and CH···π Interactions in Crystal Engineering. In *The Importance of Pi-Interactions in Crystal Engineering*; Tiekink, E. R. T.; Zukerman-Schpector, J., Eds.; John Wiley & Sons: Chichester, 2012; Chapter 2, pp 41−77.

(55) Ballester, P.; Biros, S. M. CH−π and π−π Interactions as Contributors to the Guest Binding in Reversible Inclusion and Encapsulation Complexes. In *The Importance of Pi-Interactions in Crystal Engineering*; Tiekink, E. R. T.; Zukerman-Schpector, J., Eds.; John Wiley & Sons: Chichester, 2012; Chapter 3, pp 79−107.

(56) Auras, F.; Ascherl, L.; Hakimioun, A. H.; Margraf, J. T.; Hanusch, F. C.; Reuter, S.; Bessinger, D.; Döblinger, M.; Hettstedt, C.; Karaghiosoff, K.; Herbert, S.; Knochel, P.; Clark, T.; Bein, T. Synchronized offset stacking: A concept for growing large-domain and highly crystalline 2D covalent organic frameworks. *J. Am. Chem. Soc.* **2016**, *138*, 16703−16710.

(57) Williams, J. H. Solids Formed from Aromatic Molecules. In *How Molecules Build Solids*; Morgan & Claypool: San Rafael, 2017. Chapter 11.

(58) Yao, Z.-F.; Wang, J.-Y.; Pei, J. Control of π−π stacking via crystal engineering in organic conjugated small molecule crystals. *Cryst. Growth Des.* **2018**, *18*, 7−15.

(59) Bora, P.; Saikia, B.; Sarma, B. Regulation of π···π stacking interactions in small molecule cocrystals and/or salts for physiochemical property modulation. *Cryst. Growth Des.* **2018**, *18*, 1448−1458.

(60) Chen, T.; Li, M.; Liu, J. π−π stacking interactions: A nondestructive and facile means in material engineering for bioapplications. *Cryst. Growth Des.* **2018**, *18*, 2765−2783.

(61) Li, G.-L.; Zhuo, Z.; Wang, B.; Cao, X.-L.; Su, H.-F.; Wang, W.; Huang, Y.-G.; Hong, M. Constructing π-stacked supramolecular cage based hierarchical self-assemblies via π···π stacking and hydrogen bonding. *J. Am. Chem. Soc.* **2021**, *143*, 10920−10929.

(62) Shaikh, S. R.; Gawade, R. L.; Dabke, N. B.; Dash, S. R.; Vanka, K.; Gonnade, R. G. Crystal engineering for intramolecular π−π stacking: Effect of substitution of electron-donating and electron-withdrawing groups on the molecular geometry in conformationally flexible sulfoesters and sulfonamides. *CrystEngComm* **2024**, *26*, 3557−3573.

(63) Zhang, H.-J.; Wei, Y.; Lin, J. Frustrated π-stacking. *Chem. Commun.* **2024**, *60*, 935−942.

(64) Hunter, C. A.; Sanders, J. K. M. The nature of π−π interactions. *J. Am. Chem. Soc.* **1990**, *112*, 5525−5534.

(65) Vinter, J. G. Extended electron distribution applied to the molecular mechanics of some intermolecular interactions. *J. Comput.-Aided Mol. Des.* **1994**, *8*, 653−668.

(66) Battaglia, M. R.; Buckingham, A. D.; Williams, J. H. The electric quadrupole moments of benzene and hexafluorobenzene. *Chem. Phys. Lett.* **1981**, *78*, 421−423.

(67) Wheeler, S. E.; Bloom, J. W. G. Toward a more complete understanding of noncovalent interactions involving aromatic rings. *J. Phys. Chem. A* **2014**, *118*, 6133−6147.

(68) Holtrop, F.; Visscher, K. W.; Jupp, A. R.; Slootweg, J.Steric Attraction: A Force to be Reckoned With. In *Advances in Physical Organic Chemistry*; Elsevier, 2020; Vol. *54*, pp 119−141.

(69) Saragi, R. T.; Juanes, M.; Pérez, C.; Pinacho, P.; Tikhonov, D. S.; Caminati, W.; Schnell, M.; Lesarri, A. Switching hydrogen bonding to π-stacking: The thiophenol dimer and trimer. *J. Phys. Chem. Lett.* **2021**, *12*, 1367−1373.

(70) Yamada, M. Unraveling the nature and strength of non-covalent interactions on the surface of fullerenes. *ChemPlusChem* **2023**, *88*, No. e202300062.

(71) Gao, T.; Lei, J.; Zou, S.; Wang, C.; Xu, X.; Gou, Q. Conformational equilibria and interaction preference in the complex of isoprene−maleic anhydride. *Phys. Chem. Chem. Phys.* **2023**, *25*, 27798−27804.

(72) Wang, W.; Wu, W. X.; Zhang, Y.; Jin, W. J. Perfluoroaryl···aryl interaction: The most important subset of π-hole···π bonding. *Chem. Phys. Rev.* **2024**, *5*, No. 031303.

(73) Li, J.; Peng, X.; Yin, S.; Wang, C.; Mo, Y. Metastability of the π−π stacking between the closed-shell ions of like charges. *Chin. J. Struct. Chem.* **2024**, *43*, No. 100213.

(74) Peeks, M. D.What Did Aromaticity Ever Do For Us? A User's Guide to Aromatic and Antiaromatic Molecules. In *Advances in Physical Organic Chemistry*; Elsevier, 2024; Vol. *58*, pp 1−37.

(75) Okumura, B.; Yamaguchi, E.; Komura, N.; Ohtomi, T.; Kawano, S.; Sato, H.; Katagiri, H.; Katagiri, H.; Ando, H.; Ikeda, M. Photodegradable glyco-microfibers fabricated by the self-assembly of cellobiose derivatives bearing nitrobenzyl groups. *Commun. Mater.* **2024**, *5*, No. 182.

(76) Thakuria, R.; Nath, N. K.; Saha, B. K. The nature and applications of π−π interactions: A perspective. *Cryst. Growth Des.* **2019**, *19*, 523−528.

(77) Travis, C. R.; Henriksen, H. C.; Wilkinson, J. R.; Schomburg, N. K.; Treacy, J. W.; Kean, K. M.; Houk, K. N.; Waters, M. L. WDR5 binding to histone serotonylation is driven by an edge-face aromatic interaction with unexpected electrostatic effects. *J. Am. Chem. Soc.* **2024**, *146*, 27451−27459.

(78) Adams, H.; Carver, F. J.; Hunter, C. A.; Morales, J. C.; Seward, E. M. Chemical double-mutant cycles for the measurement of weak intermolecular interactions: Edge-to-face aromatic interactions. *Angew. Chem., Int. Ed. Engl.* **1996**, *35*, 1542−1544.

(79) Adams, H.; Blanco, J.-L. J.; Chessari, G.; Hunter, C. A.; Low, C. M. R.; Sanderson, J. M.; Vinter, J. G. Quantitative determination of intermolecular interactions with fluorinated aromatic rings. *Chem. - Eur. J.* **2001**, *7*, 3494−3503.

(80) Carver, F. J.; Hunter, C. A.; Livingstone, D. J.; McCabe, J. F.; Seward, E. M. Substituent effects on edge-to-face aromatic interactions. *Chem. - Eur. J.* **2002**, *8*, 2847−2859.

(81) Cockroft, S. L.; Hunter, C. A.; Lawson, K. R.; Perkins, J.; Urch, C. J. Electrostatic control of aromatic stacking interactions. *J. Am. Chem. Soc.* **2005**, *127*, 8594−8595.

(82) Cockroft, S. L.; Perkins, J.; Zonta, C.; Adams, H.; Spey, S. E.; Low, C. M. R.; Vinter, J. G.; Lawson, K. R.; Urch, C. J.; Hunter, C. A.

Substituent effects on aromatic stacking interactions. *Org. Biomol. Chem.* **2007**, *5*, 1062−1080.

(83) Schneider, H.-J. Requirements for quantifications of weak intermolecular interactions from equilibrium studies with supramolecular complexes. *Angew. Chem., Int. Ed. Engl.* **1997**, *36*, 1072−1073.

(84) Kim, E.-i.; Paliwal, S.; Wilcox, C. S. Measurements of molecular electrostatic field effects in edge-to-face aromatic interactions and CH-π interactions with implications for protein folding and molecular recognition. *J. Am. Chem. Soc.* **1998**, *120*, 11192−11193.

(85) Martínez, A. G.; Osío Barcina, J. O.; de Fresno Cerezo, A. Influence of highly preorganised 7,7-diphenylnobornane in the free energy of edge-to-face aromatic interactions. *Chem. - Eur. J.* **2001**, *7*, 1171−1175.

(86) Gung, B. W.; Xue, X.; Zou, Y. Enthalpy (ΔH) and entropy (ΔS) for π-stacking interactions in near-sandwich configurations: Relative importance of electrostatic, dispersive, and charge-transfer effects. *J. Org. Chem.* **2007**, *72*, 2469−2475.

(87) Rashkin, M. J.; Waters, M. L. Unexpected substituent effects in offset $\pi-\pi$ stacked interactions in water. *J. Am. Chem. Soc.* **2002**, *124*, 1860−1861.

(88) Snyder, S. E.; Huang, B.-S.; Chen, Y.-T.; Lin, H.-S.; Carey, J. R. A simple chiral recognition system to investigate substituent effects on $\pi-\pi$ interactions. *Org. Lett.* **2012**, *14*, 3442−3445.

(89) Snyder, S. E.; Huang, B.-S.; Chu, Y. W.; Lin, H.-S.; Carey, J. R. The effects of substituents on the geometry of $\pi-\pi$ interactions. *Chem. - Eur. J.* **2012**, *18*, 12663−12671.

(90) Hwang, J.; Li, P.; Carroll, W. R.; Smith, M. D.; Pellechia, P. J.; Shimizu, K. D. Additivity of substituent effects in aromatic stacking interactions. *J. Am. Chem. Soc.* **2014**, *136*, 14060−14067.

(91) Harder, M.; Corrales, M. A. C.; Trapp, N.; Kuhn, B.; Diederich, F. Rebek imide platforms as model systems for the investigation of weak intermolecular interactions. *Chem. - Eur. J.* **2015**, *21*, 8455−8463.

(92) Hwang, J.; Li, P.; Vik, E. C.; Karki, I.; Shimizu, K. D. Study of through-space substituent-π interactions using *N*-phenylimide molecular balances. *Org. Chem. Front.* **2019**, *6*, 1266−1271.

(93) Burns, R. J.; Mati, I. K.; Muchowska, K. B.; Adam, C.; Cockroft, S. L. Quantifying through-space substituent effects. *Angew. Chem., Int. Ed.* **2020**, *59*, 16717−16724.

(94) Karki, S.; Jalife, S.; Wang, X.; Lin, Y.-H.; Wu, J. I.; Miljanić, O. Š. Columnar organization of nonalternant fluorinated dehydrobenzannulenes. *Chem. - Eur. J.* **2024**, *30*, No. e202402913.

(95) Salonen, L. M.; Ellermann, M.; Diederich, F. Aromatic rings in chemical and biological recognition: Energetics and structures. *Angew. Chem., Int. Ed.* **2011**, *50*, 4808−4842.

(96) Li, S.; Xu, Y.; Shen, Q.; Liu, X.; Lu, J.; Chen, Y.; Lu, T.; Luo, C.; Luo, X.; Zheng, M.; Jiang, H. Non-covalent interactions with aromatic rings: Current understanding and implications for rational drug design. *Curr. Pharm. Des.* **2013**, *19*, 6522−6533.

(97) Garcia, A. M.; Determan, J. J.; Janesko, B. G. Tunable fictitious substituent effects on the $\pi-\pi$ interactions of substituted sandwich benzene dimers. *J. Phys. Chem. A* **2014**, *118*, 3344−3350.

(98) Tehrani, Z. A.; Kim, K. S. Functional molecules and materials by π-interaction based quantum theoretical design. *Int. J. Quantum Chem.* **2016**, *116*, 6222−6633.

(99) Quinteros-Lama, H.; Llovell, F.; Wisniak, J. The polyazeotropic behaviour of the benzene plus hexafluorobenzene system revisited. *J. Chem. Thermodyn.* **2017**, *113*, 340−349.

(100) Cockcroft, J. K.; Rosu-Finsen, A.; Fitch, A. N.; Williams, J. H. The temperature dependence of C-H···F-C interactions in benzene:hexafluorobenzene. *CrystEngComm* **2018**, *20*, 6677−6682.

(101) Mandal, A.; Choudhury, A.; Iyer, P. K.; Mal, P. Charge transfer versus arene-perfluoroarene interactions in modulation of optical and conductivity properties in cocrystals of 2,7-di-tert-butylpyrene. *J. Phys. Chem. C* **2019**, *123*, 18198−18206.

(102) Rasheed, N.; Galant, N. J.; Csizmadia, I. G. Structure-activity relationship of dicoumarol derivatives as anti-*Staphlococcus aureas* (staph infection) agents. *Anti-Infect. Agents* **2019**, *17*, 93−98.

(103) Chakraborty, G.; Bardhan, S.; Ghosh, S.; Saha, S. K. Relevance of π-stacking in tuning the neighboring structural pattern of soft nanoaggregates. *J. Mol. Liq.* **2020**, *317*, No. 114013.

(104) D'Avino, G.; Duhm, S.; Valle, R. G. D.; Heimel, G.; Oehzelt, M.; Kera, S.; Ueno, N.; Beljonne, D.; Salzmann, I. Electrostatic interactions shape molecular organization and electronic structure of organic semiconductor blends. *Chem. Mater.* **2020**, *32*, 1261−1271.

(105) Melikova, S. M.; Voronin, A. P.; Panek, J.; Frolov, N. E.; Shishkina, A. V.; Rykounov, A. A.; Tretyakov, P. Y.; Vener, M. V. Interplay of π-stacking and inter-stacking interactions in two-component crystals of neutral closed-shell aromatic compounds: Periodic DFT study. *RSC Adv.* **2020**, *10*, 27899−27910.

(106) Kaczmarek-Kędziera, A.; Żuchowski, P. S.; Kędziera, D. Nature of intermolecular interaction in squaraine dimers. *Sci. Rep.* **2020**, *10*, No. 19670.

(107) Lee, G. Y.; Hu, E.; Rheingold, A. L.; Houk, K. N.; Sletten, E. M. Arene-perfluoroarene interactions in solution. *J. Org. Chem.* **2021**, *86*, 8425−8436.

(108) Houghton, A.; Appelhagen, I.; Martin, C. Natural blues: Structure meets function in anthocyanins. *Plants* **2021**, *10*, No. 726.

(109) Sharber, S. A.; Mullin, W. J.; Thomas, S. W., III Bridging the void: Halogen bonding and aromatic interactions to program luminescence and electronic properties of π-conjugated materials in the solid state. *Chem. Mater.* **2021**, *33*, 6640−6661.

(110) Dharmarwardana, M.; Otten, B. M.; Ghimire, M. M.; Arimilli, B. S.; Williams, C. M.; Boateng, S.; Lu, Z.; McCandless, G. T.; Gassensmith, J. J.; Omary, M. A. Strong π−stacking causes unusually large anisotropic thermal expansion and thermochroism. *Proc. Natl. Acad. Sci. U.S.A.* **2021**, *118*, No. e2106572118.

(111) Daso, R. E.; Mitchell, S. M.; Lebedenko, C. G.; Heise, R. M.; Banerjee, I. A. Exploring the interactions of ionic liquids with bio-organic amphiphiles using computational approaches. *ACS Omega* **2021**, *6*, 32460−32474.

(112) Akashah, M. H. N.; Sahudin, M. R.; Rani, A. R.; Scully, P. J.; Makhsin, S. R.; Al-Douri, Y. Chemical Properties of Graphene. In*Graphene, Nanotubes and Quantum Dots-Based Nanotechnology: Fundamentals and Applications*; Al-Douri, Y., Ed.; Elsevier: Cambridge, 2022; Chapter 3, pp 43−67.

(113) Patarroyo, M. E.; Bermudez, A.; Alba, M. P.; Patarroyo, M. A.; Suarez, C.; Aza-Conde, J.; Moreno-Vranich, A.; Vanegas, M. Stereo electronic principles for selecting fully-protective, chemically-synthesised malaria vaccines. *Front. Immunol.* **2022**, *13*, No. 926680.

(114) Zhou, G.; Zhang, M.; Xu, J.; Yang, Y.; Hao, T.; Zhu, L.; Zhou, L.; Zhu, H.; Zou, Y.; Wei, G.; Zhang, Y.; Liu, F. Spontaneous carrier generation and low recombination in high-efficiency non-fullerene solar cells. *Energy Environ. Sci.* **2022**, *15*, 3483−3493.

(115) Ridgway, H.; Moore, G. J.; Mavromoustakos, T.; Tsiodras, S.; Ligielli, I.; Kelaidonis, K.; Chasapis, C. T.; Gaganec, L. K.; Zulli, A.; Apostolopoulos, V.; Petty, R.; Karakasiliotis, I.; Gorgoulis, V. G.; Matsoukas, J. M. Discovery of a new generation of angiotensin receptor blocking drugs: Receptor mechanisms and in silico binding to enzymes relevant to SARS-CoV-2. *Comput. Struct. Biotechnol. J.* **2022**, *20*, 2091−2111.

(116) Roesner, E. K.; Asheghali, D.; Kirillova, A.; Strauss, M. J.; Evans, A. M.; Becker, M. L.; Dichtel, W. R. Arene-perfluoroarene interactions confer enhanced mechanical properties to synthetic nanotubes. *Chem. Sci.* **2022**, *13*, 2475−2480.

(117) Ghamartale, A.; Rezaei, N.; Zendehboudi, S. Alternation of asphaltene binding arrangement in the presence of chemical inhibitors: Molecular dynamics simulation strategy. *Fuel* **2023**, *336*, No. 127001.

(118) Alhunayhin, S. M. N.; Bushby, R. J.; Cammidge, A. N.; Samman, S. S. Triphenylene discotic liquid crystals: Biphenyls, synthesis, and the search for nematic systems. *Liq. Cryst.* **2023**, *51*, 1333−1344.

(119) Ismael, A. K.; Taha, T. A. M.; Al-Jobory, A. Three distinct conductance states in polycyclic aromatic hydrocarbon derivatives. *R. Soc. Open Sci.* **2024**, *11*, No. 231734.

(120) Chiñas-Rojas, L. E.; Domínguez, J. E.; Herrera, L. A. A.; González-Jiménez, F. E.; Colorado-Peralta, R.; Altaif, J. A. A.; Villanueva, J. M. R. Exploring synthesis strategies and interactions between MOFs and drugs for controlled drug loading and release, characterizing interactions through advanced techniques. *ChemMedChem* **2024**, *19*, No. e202400144.

(121) Zhang, S.; Chen, A.; An, Y.; Li, Q. Arene-perfluoroarene interaction: Properties, constructions, and applications in materials science. *Matter* **2024**, *7*, 3317−3350.

(122) Anjum, N.; Oba, S.; Hiaki, T.; Hsieh, C.-J.; Chen, C.-C. Thermodynamic modeling of double azeotropy systems. *Fluid Phase Equilib.* **2024**, *578*, No. 113993.

(123) Wheeler, S. E.; Houk, K. N. Substituent effects in the benzene dimer are due to direct interactions of the substituents with the unsubstituted benzene. *J. Am. Chem. Soc.* **2008**, *130*, 10854−10855.

(124) Wheeler, S. E.; Houk, K. N. Through-space effects of substituents dominate molecular electrostatic potentials of substituted arenes. *J. Chem. Theory Comput.* **2009**, *5*, 2301−2312.

(125) Wheeler, S. E.; Houk, K. N. Origin of substituent effects in edge-to-face aryl-aryl interactions. *Mol. Phys.* **2009**, *107*, 749−760.

(126) Wheeler, S. E. Local nature of substituent effects in stacking interactions. *J. Am. Chem. Soc.* **2011**, *133*, 10262−10274.

(127) Raju, R. K.; Bloom, J. W. G.; Wheeler, S. E. Broad transferability of substituent effects in π-stacking interactions provides new insights into their origin. *J. Chem. Theory Comput.* **2013**, *9*, 3479−3490.

(128) Cozzi, F.; Siegel, J. S. Interaction between stacked aryl groups in 1,8-diarylnaphthalenes: Dominance of polar/π over charge-transfer effects. *Pure Appl. Chem.* **1995**, *67*, 683−689.

(129) Cozzi, F.; Cinquini, M.; Annunziata, R.; Dwyer, T.; Siegel, J. S. Polar/π interactions between stacked aryls in 1,8-diarylnaphthalenes. *J. Am. Chem. Soc.* **1992**, *14*, 5729−5733.

(130) Cozzi, F.; Cinquini, M.; Annuziata, R.; Siegel, J. S. Dominance of polar/ π over charge-transfer effects in stacked phenyl interactions. *J. Am. Chem. Soc.* **1993**, *115*, 5330−5331.

(131) Cozzi, F.; Ponzini, F.; Annunziata, R.; Cinquini, M.; Siegel, J. S. Polar interactions between stacked π systems in fluorinated 1,8-diarylnaphthalenes: Importance of quadrupole moments in molecular recognition. *Angew. Chem., Int. Ed. Engl.* **1995**, *34*, 1019−1020.

(132) Cozzi, F.; Annunziata, R.; Benaglia, M.; Cinquini, M.; Raimondi, L.; Baldridge, K. K.; Siegel, J. S. Through-space interactions between face-to-face, center-to-edge oriented arenes: Importance of polar-π effects. *Org. Biomol. Chem.* **2003**, *1*, 157−162.

(133) Cozzi, F.; Annunziata, R.; Benaglia, M.; Baldridge, K. K.; Aguirre, G.; Estrada, J.; Sritana-Anant, Y.; Siegel, J. S. Through-space interactions between parallel-offset arenes at the van der Waals distance: 1,8-diarylbiphenylene syntheses, structure and QM computations. *Phys. Chem. Chem. Phys.* **2008**, *10*, 2686−2694.

(134) Wheeler, S. E.; Houk, K. N. Substituent effects in cation/π interactions and electrostatic potentials above the centers of substituted benzenes are due primarily to through-space effects of the substituents. *J. Am. Chem. Soc.* **2009**, *131*, 3126−3127.

(135) Arnstein, S. A.; Sherrill, C. D. Substituent effects in parallel-displaced $\pi-\pi$ interactions. *Phys. Chem. Chem. Phys.* **2008**, *10*, 2646−2655.

(136) Parrish, R. M.; Sherrill, C. D. Quantum-mechanical evaluation of the $\pi-\pi$ versus substituent-π interactions in π stacking: Direct evidence for the Wheeler-Houk picture. *J. Am. Chem. Soc.* **2014**, *136*, 17386−17389.

(137) Ringer, A. L.; Sinnokrot, M. O.; Lively, R. P.; Sherrill, C. D. The effect of multiple substituents on sandwich and T-shaped $\pi-\pi$ interactions. *Chem. - Eur. J.* **2006**, *12*, 3821−3828.

(138) Clements, A.; Lewis, M. Arene-cation interactions of positive quadrupole moment aromatics and arene-anion interactions of negative quadrupole moment aromatics. *J. Phys. Chem. A* **2006**, *110*, 12705−12710.

(139) Wheeler, S. E.; Houk, K. N. Are anion/ π interactions actually a case of simple charge-dipole interactions? *J. Phys. Chem. A* **2010**, *114*, 8658−8664.

(140) Gharahcheshmeh, M. H.; Robinson, M. T.; Gleason, E. F.; Gleason, K. K. Optimizing the optoelectronic properties of face-on oriented poly(3,4-ethylenedioxythiophene) via water-assisted oxidative chemical vapor deposition. *Adv. Funct. Mater.* **2020**, *31*, No. 2008712.

(141) Kaplan, I. G. *Intermolecular Interactions: Physical Picture, Computational Methods and Model Potentials*; John Wiley & Sons: Chichester, United Kingdom, 2006.

(142) Stone, A. J. Physical Basis of Intermolecular Interactions. In *Non-Covalent Interactions in Quantum Chemistry and Physics*; de la Roza, A. O.; DiLabio, G. A., Eds.; Elsevier: Amsterdam, 2017; Chapter 1, pp 3−26.

(143) Szalewicz, K.; Jeziorski, B. Physical mechanisms of intermolecular interactions from symmetry-adapted perturbation theory. *J. Mol. Model.* **2022**, *28*, No. 273.

(144) Misquitta, A. J. Charge transfer from regularized symmetry-adapted perturbation theory. *J. Chem. Theory Comput.* **2013**, *9*, 5313−5326.

(145) Řezáč, J.; de la Lande, A. Robust, basis-set independent method for the evaluation of charge-transfer energy in noncovalent complexes. *J. Chem. Theory Comput.* **2015**, *11*, 528−537.

(146) Lao, K. U.; Herbert, J. M. Energy decomposition analysis with a stable charge-transfer term for interpreting intermolecular interactions. *J. Chem. Theory Comput.* **2016**, *12*, 2569−2582.

(147) Herbert, J. M.; Carter-Fenk, K. Electrostatics, charge transfer, and the nature of the halide-water hydrogen bond. *J. Phys. Chem. A* **2021**, *125*, 1243−1256.

(148) Lao, K. U.; Herbert, J. M. Accurate intermolecular interactions at dramatically reduced cost: XPol+SAPT with empirical dispersion. *J. Phys. Chem. Lett.* **2012**, *3*, 3241−3248.

(149) Lao, K. U.; Herbert, J. M. Accurate and efficient quantum chemistry calculations of noncovalent interactions in many-body systems: The XSAPT family of methods. *J. Phys. Chem. A* **2015**, *119*, 235−253.

(150) Lao, K. U.; Herbert, J. M. Atomic orbital implementation of extended symmetry-adapted perturbation theory (XSAPT) and benchmark calculations for large supramolecular complexes. *J. Chem. Theory Comput.* **2018**, *14*, 2955−2978.

(151) Lao, K. U.; Herbert, J. M. Symmetry-adapted perturbation theory with Kohn-Sham orbitals using non-empirically tuned, long-range-corrected density functionals. *J. Chem. Phys.* **2014**, *140*, No. 044108.

(152) Nguyen, B. D.; Chen, G. P.; Agee, M. M.; Burow, A. M.; Tang, M.; Furche, F. Divergence of many-body perturbation theory for noncovalent interactions of large molecules. *J. Chem. Theory Comput.* **2020**, *16*, 2258−2273.

(153) Parker, T. M.; Burns, L. A.; Parrish, R. M.; Ryno, A. G.; Sherrill, C. D. Levels of symmetry adapted perturbation theory (SAPT). I. Efficiency and performance for interaction energies. *J. Chem. Phys.* **2014**, *140*, No. 094106.

(154) Hohenstein, E. G.; Sherrill, C. D. Wavefunction methods for noncovalent interactions. *WIREs Comput. Mol. Sci.* **2012**, *2*, 304−326.

(155) Patkowski, K. Recent developments in symmetry-adapted perturbation theory. *WIREs Comput. Mol. Sci.* **2020**, *10*, No. e1452.

(156) Ambrosetti, A.; Reilly, A. M.; DiStasio, R. A., Jr.; Tkatchenko, A. Long-range correlation energy calculated from coupled atomic response functions. *J. Chem. Phys.* **2014**, *140*, No. 18A508.

(157) Liu, K.-Y.; Carter-Fenk, K.; Herbert, J. M. Self-consistent charge embedding at very low cost, with application to symmetry-adapted perturbation theory. *J. Chem. Phys.* **2019**, *151*, No. 031102.

(158) Carter-Fenk, K.; Lao, K. U.; Liu, K.-Y.; Herbert, J. M. Accurate and efficient *ab initio* calculations for supramolecular complexes: Symmetry-adapted perturbation theory with many-body dispersion. *J. Phys. Chem. Lett.* **2019**, *10*, 2706−2714.

(159) Gray, M.; Herbert, J. M. Simplified tuning of long-range corrected density functionals for symmetry-adapted perturbation theory. *J. Chem. Phys.* **2021**, *155*, No. 034103.

(160) Gray, M.; Herbert, J. M. Comprehensive basis-set testing of extended symmetry-adapted perturbation theory and assessment of

mixed-basis combinations to reduce cost. *J. Chem. Theory Comput.* **2022**, *18*, 2308−2330.

(161) Shahbaz, M.; Szalewicz, K. Do semilocal density-functional approximations recover dispersion energies at small intermonomer separations? *Phys. Rev. Lett.* **2018**, *121*, No. 113402.

(162) Shahbaz, M.; Szalewicz, K. Evaluation of methods for obtaining dispersion energies used in density functional calculations of intermolecular interactions. *Theor. Chem. Acc.* **2019**, *138*, No. 25.

(163) Gray, M.; Herbert, J. M.Density Functional Theory for Van der Waals Complexes: Size Matters. In *Annual Reports in Computational Chemistry*; Elsevier, 2024; Vol. *20*, pp 1−61.

(164) Epifanovsky, E.; Gilbert, A. T. B.; Feng, X.; et al. Software for the frontiers of quantum chemistry: An overview of developments in the Q-Chem 5 package. *J. Chem. Phys.* **2021**, *155*, No. 084801.

(165) Rowland, R. S.; Taylor, R. Intermolecular nonbonded contact distances in organic crystal structures: Comparison with distances expected from van der Waals radii. *J. Phys. Chem. A* **1996**, *100*, 7384−7391.

(166) Falcioni, F.; Symons, B. C. B.; Popelier, P. L. A.REG-MULTI: Lifting the Veil on Electrostatic Interactions. In *Advances in Quantum Chemistry*; Elsevier, 2023; Vol. *88*, pp 305−328.

(167) Franklin, R. E. The structure of graphitic carbon. *Acta Crystallogr.* **1951**, *4*, 253−261.

(168) Tsuzuki, S.; Honda, K.; Uchimaru, T.; Mikami, M.; Tanabe, K. Origin of attraction and directionality of the π/π interaction: Model chemistry calculations of benzene dimer interaction. *J. Am. Chem. Soc.* **2002**, *124*, 104−112.

(169) Hunter, C. A. Arene-arene interactions: Electrostatic or charge transfer? *Angew. Chem., Int. Ed. Engl.* **1993**, *32*, 1584−1586.

(170) Tsuzuki, S. Interactions with Aromatic Rings. In *Intermolecular Forces and Clusters I*; Wales, D. J., Ed.; Springer-Verlag: Berlin, 2005; *Structure and Bonding*, Vol. *115*, pp 149−193.

(171) Hansch, C.; Leo, A.; Taft, R. W. A survey of Hammett substituent constants and resonance field parameters. *Chem. Rev.* **1991**, *91*, 165−195.

(172) Tsuzuki, S.; Mikami, M.; Yamada, S. Origin of attraction, magnitude, and directionality of interactions in benzene complexes with pyridinium cations. *J. Am. Chem. Soc.* **2007**, *129*, 8656−8662.

(173) Hohenstein, E. G.; Sherrill, D. C. Effects of heteroatoms on aromatic $\pi-\pi$ interactions: Benzene-pyridine and pyridine dimer. *J. Phys. Chem. A* **2009**, *113*, 878−886.

(174) *Handbook of Thiophene-Based Materials: Applications in Organic Electronics and Photonics*; Perepichka, I. F.; Perepichka, D. F., Eds.; John Wiley & Sons, Ltd.: Chichester, 2009.

(175) Smith, D. W. A simple molecular orbital treatment of the barrier to internal rotation in the ethane molecule. *J. Chem. Educ.* **1998**, *75*, 907−909.

(176) Tsuzuki, S.; Honda, K.; Uchimaru, T.; Mikami, M. Intermolecular interactions of nitrobenzene-benzene complex and nitrobenzene dimer: Significant stabilization of slipped-parallel orientation by dispersion interaction. *J. Chem. Phys.* **2006**, *125*, No. 124304.

(177) Rohrdanz, M. A.; Martins, K. M.; Herbert, J. M. A long-range-corrected density functional that performs well for both ground-state properties and time-dependent density functional theory excitation energies, including charge-transfer excited states. *J. Chem. Phys.* **2009**, *130*, No. 054112.

(178) Ohio Supercomputer Center http://osc.edu/ark:/19495/f5s1ph73. (accessed December 20, 2024).